J. Electrochem. Sci. Eng. **9(4)** (2019) 281-310; http://dx.doi.org/10.5599/jese.665

Open Access: ISSN 1847-9286
https://pub.iapchem.org/ojs/index.php/JESE

Review

Platinum utilization in proton exchange membrane fuel cell and direct methanol fuel cell

Madhavi Bandapati[1], Sanket Goel[2] and Balaji Krishnamurthy[1,✉]

[1]*Department of Chemical Engineering, BITS-Pilani, Hyderabad Campus, Hyderabad-500078, India*
[2]*Department of Electrical and Electronics Engineering, BITS-Pilani, Hyderabad Campus, Hyderabad-500078, India*

Corresponding author: balaji@hyderabad.bits-pilani.ac.in; balaji.krishb1@gmail.com;
Tel.: +91-040-663-03552

Received: February 15, 2018; Revised: March 22, 2019; Accepted: March 25, 2019

Abstract

Proton exchange membrane fuel cell (PEMFC) and direct methanol fuel cell (DMFC) are increasingly used as substitutes to conventional energy systems. Their compact design, high energy density and efficient energy-conversion offer several advantages over existing energy systems with potential for use in a variety of applications. However, performance, robustness and cost are the key challenges to overcome before fuel cells can be commercialized. Even though the use of platinum (Pt) and platinum group metal (PGM) alloy catalysts provide higher performance and durability, they are at the same time the largest cost components which need to be addressed. This paper reviews different approaches adopted to enhance Pt utilization such as reducing Pt loading, decreasing Pt particle size, developing Pt free metallic alloy catalyst, improving Pt dispersion, developing membrane electrode assembly (MEA) fabrication methods, increasing mass-transport at the electrode surface and modifying the catalyst support materials. Finally, the performance optimization efforts for Pt utilization are summarized with insights into probable directions of future research in this area.

Keywords

Electrochemical active surface area; hydrogen adsorption; CO stripping; catalyst particle size; catalyst loading; catalyst dispersion; catalyst support

Introduction

Over the last two decades, proton exchange membrane fuel cell (PEMFC) and direct methanol fuel cell (DMFC) have been extensively studied and are emerging as potential systems as they provide clean energy and are commercially viable [1]. They possess a series of highly advantages features such as low operating temperature (<100 °C), high efficiency, sustainability at high current

density, development of catalyst material for hydrogen generation, 10-100 fold reduction of the catalyst loading, multiple options for membrane electrode assembly (MEA) fabrication, manufacturing and synthesis process for gas diffusion layer (GDL) and membranes, development in thermal and water management, compactness, potential for low volume and weight, long stack life, fast start-up and suitability for discontinuous operation [2-4].

In the recent years, leveraging these advantages, automobile and fuel cell (FC) manufacturers are moving towards commercialization from a demonstration phase. This is carried out through development of suitable catalysts, introduction of zero emission vehicles and development of prototype vehicles that have adopted FC systems. However, several technological challenges and cost reduction still need to be overcome. The primary approaches towards addressing these challenges include reducing the precious metal catalyst loading with controlled particle deposition through improved electrode preparation methods, optimizing the MEA, enhancing the tolerance of MEA to high temperature to promote higher degrees of electro-catalysis, exploring non-platinum based electrode materials [5-7].

Platinum (Pt) or Pt-alloys such as PtRu, PtCo, PtNi, PtFe, PtV, PtMn, PtCr are the most suitable electrocatalysts for PEMFCs and DMFCs as they have low overpotential values, high catalytic activities and also ability to tolerate the harsh acidic surroundings inside FC. Pt is a less abundant and expensive noble metal that contributes as much as 50 % (even at 1.7 % of Pt) to the total cost of fuel cell. In addition, Pt utilization is quite low with only 25-35 % utilized for electroactivity [8-10].

The limited supply and high cost of Pt necessitate its optimal utilization and reduction in Pt loading. Table 1 illustrates the status and long term goals set by the U.S. Department of Energy for Pt utilization with Pt loading targets. As a result, optimizing Pt utilization in order to reduce cost has been the primary focus of much research in this field [11-13].

Table 1. *Platinum metal content status and targets [13]*

Characteristics	**2011 status**	**Targets**	
		2017	**2020**
Platinum group metal (PGM) total content (both electrodes), g kW^{-1}	0.19	0.125	0.125
PGM total loading, mg m^{-2}	0.15	0.125	0.125
Loss in initial catalytic activity, wt%	48	40	40
Electrocatalyst support stability, wt%	10	10	10
Mass activity, A mg_{Pt}^{-1}	0.24	0.44	0.44
Non-Pt catalyst activity per volume of supported catalyst, A cm^{-3}	60	300	300

In order to improve Pt utilization efficiency, the electrocatalysts need to be developed with the reduced Pt loading and increased Pt active sites. The active research approaches explored towards enhancement of effective Pt utilization in PEMFC and DMFC electrodes are grouped in following categories [14,15]:

- Reducing the electrocatalysts loading in fuel cell electrodes.
- Developing novel nano-structured thin-film Pt by decreasing the electrocatalysts nanoparticle size
- Reducing Pt dependence by developing metallic alloys and Pt-free electrocatalysts.
- Improving electrocatalysts dispersion by using novel fabrication methods.
- Developing MEA fabrication methods to enable better catalyst dispersion and utilization.
- Using new techniques to increase mass-transport at the fuel cell electrode surface.
- Improving the performance of carbonaceous electrocatalysts support and exploring novel non-carbonaceous electrocatalysts support materials.

(cc) BY

Although Pt is the catalyst commonly used for both anode and cathode in PEMFCs, the oxygen reduction reaction (ORR) at cathode is more complex with sluggish reaction kinetics, thus requiring higher Pt loading, typically several times higher than that of anode. In addition, the hydrogen oxidation reaction (HOR) on the DMFC anode catalyst suffers from high over potential. This has triggered researchers to explore optimization of Pt catalyst including the synthesis of catalysts that are more active and less expensive than Pt [16,17].

This paper focuses on various approaches, already taken by researchers to optimize Pt utilization for cathode of PEMFC and both electrodes of DMFC to reduce the cost and improve the performance and durability of PEMFCs and DMFCs. Catalyst utilization can also be represented in terms of mass activity and specific activity. As catalyst utilization is a surface phenomenon [18], the progress made in this area has been presented by considering electrochemical active surface area (ECSA), as the benchmark parameter across various research approaches over a period of time. The calculation procedure of this parameter is briefly described in the following section.

In addition, fuel cell performance can also be increased by increasing specific activity of the catalyst by alloying or shaping. Specific activity (SA) is the ratio of the kinetic current to the real surface area of the catalyst. Nevertheless, in the case of nanostructures the real surface area is significantly greater than geometric and can be determined using CO stripping [21]. However, discussing specific activity of the catalyst is beyond the scope of this review.

Measuring platinum utilization efficiency

Platinum utilization (PtUt) is the amount of exposed Pt atoms available for catalytic reaction among those dispersed on the electrode. As catalyst utilization is a surface phenomenon, the surface and the specific surface area are considered as critical factors for measurement. Here, electrochemical active surface area (ECSA) is considered as a measure of Pt utilization. A comparison of ECSA with geometrical specific surface area (GSA) tells the number of electrochemically active Pt surface atoms. Therefore, the ratio of ECSA to GSA is considered as a measure of PtUt [19,20].

$$\text{PtUt, \%} = [\text{ECSA/GSA}] \times 100 \quad (1)$$

Electrochemical active surface area (ECSA)

ECSA is a measure of the number of electroactive Pt sites on the surface of the catalyst on which reaction occurs and is sometimes called the intrinsic Pt catalyst surface area. Numerous methods are available in the literature to calculate ECSA of Pt catalysts. In the context of this review, two primary methods, H-adsorption ($ECSA_H$) and CO stripping ($ECSA_{CO}$) used for measuring ECSA are explained below [21].

H-adsorption ($ECSA_H$)

$ECSA_H$ of Pt catalyst, reported in $m^2 g_{Pt}^{-1}$ units, is determined conventionally from hydrogen under-potential deposition (HUPD) reaction, which can be expressed as [22]:

$$Pt + H^+ + e^- \rightleftarrows Pt\text{-}H_{ads} \quad (2)$$

Figure 1 shows a typical hydrogen electrosorption/desorption voltammetric profile for the polycrystalline Pt electrode in 0.5 M H_2SO_4. Characteristic peaks between 0.0 and ~ 0.2 V are attributed to the atomic hydrogen desorption/adsorption at Pt surface and $ECSA_H$ can be determined by:

$$ECSA_H = (100\ Q_H) / (Q_{H(ref)}\ m) \quad (3)$$

In Eq. (3), Q_H / μC is the charge calculated by integrating the area under the cyclic voltammetry (CV) curve (Figure 1) within the potential range of hydrogen desorption, $Q_{H(ref)}$ is the charge corresponding to formation of the monolayer of adsorbed hydrogen on the polycrystalline Pt given as 210 μC cm^{-2}, and *m* is the mass of Pt loading (mg) that indicates the amount of Pt at the working electrode [23,24].

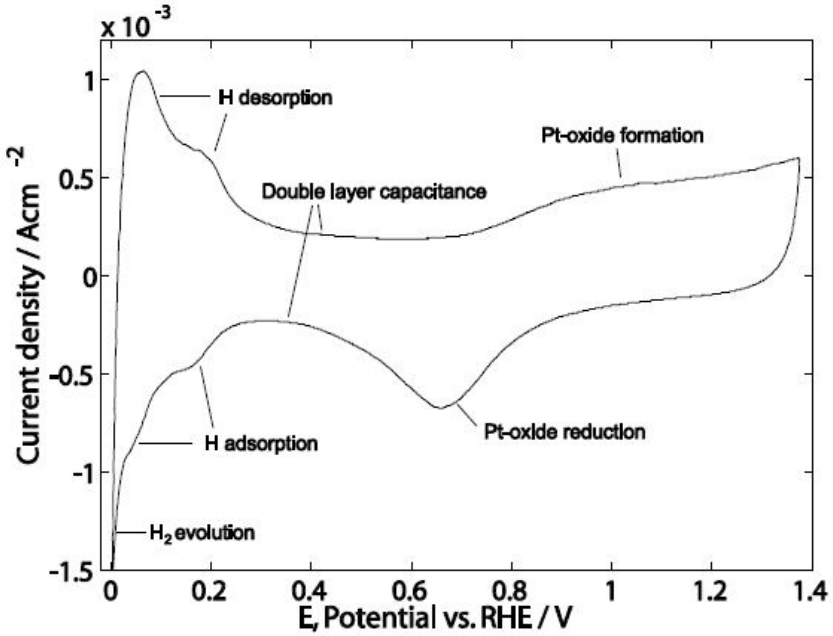

Figure 1. *Typical hydrogen adsorption/desorption voltammetry profile for polycrystalline Pt electrode in 0.5 M H_2SO_4 at room temperature at 100 mVs^{-1} [21]*

When electrodes are fabricated with the polymer electrolyte membrane (PEM), however, all Pt active sites are not available for electrochemical reaction. This may be due to an improper contact of Pt particles with the solid polymer electrolyte or to electrical insulation between Pt particles caused by a thin film of the electrically non-conducting polymer electrolyte. In such case, the ECSA measured by CV in solid polymer electrolyte is denoted as $ECSA_{MEA}$ which is called as driven – cell mode [25]. This value may be smaller than ECSA. The ratio of ECSA and $ECSA_{MEA}$ is termed as MEA platinum utilization [81].

CO stripping

The most commonly used anode catalyst for DMFC is platinum-ruthenium (PtRu). The ECSA and performance of the prepared PtRu anode catalysts for DMFC are measured by means of CO stripping method.

Pre-adsorbed carbon monoxide (CO_{ad}) oxidation can be calculated using CO adsorption removal voltammogram (Figure 2) at a particular scan rate. Gaseous CO can be purged into the cell to permit complete CO adsorption onto the electrocatalyst while maintaining a steady voltage. The surplus CO can be removed by nitrogen gas [26].

The following reactions occur on the platinum surface for methanol oxidation:

$$CH_3OH + Pt \rightarrow CO_{ad}\text{-}Pt + 4H^+ + 4e^- \quad (4a)$$

$$Pt + CO_{ad}\text{-}Pt + H_2O \rightarrow CO_{ad}\text{-}Pt + H^+ + OH_{ad}\text{-}Pt + e^- \rightarrow 2Pt + 2H^+ + CO_2 + 2e^- \quad (4b)$$

For PtRu, the equation for methanol oxidation is as follows:

$$CH_3OH + PtRu \rightarrow CO_{ad}\text{-}PtRu + 4e^- + 4H^+ \quad (5a)$$

$$CO_{ad}\text{-}PtRu + H_2O \rightarrow CO_{ad}\text{-}PtRu\text{-}OH_{ad} + e^- + H^+ \rightarrow PtRu + CO_2 + 2e^- + 2H^+ \quad (5b)$$

(cc) BY

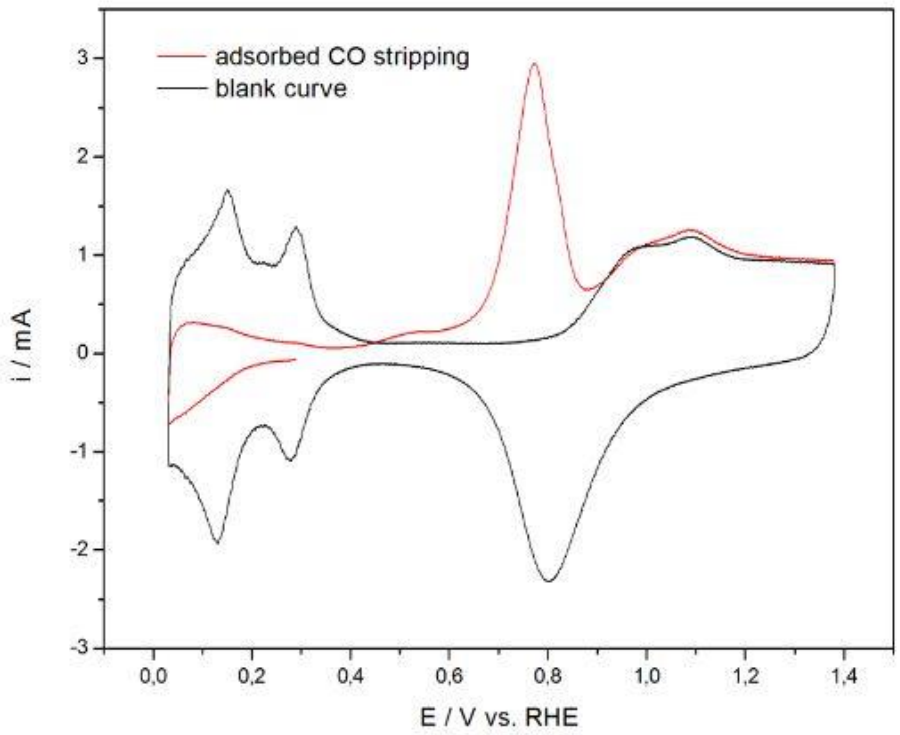

Figure 2. *CO stripping current (red line) recorded at 500 mVs^{-1} scan rate for polycrystalline Pt electrode in 0.5 M H_2SO_4 at 298 K together with a blank curve (black line). CO adsorption at 0.29 V vs. RHE for 20 min [21]*

As the charge of the CO oxidation peak is taken as two electrons per CO molecule, the resulting charge is approximately double of that corresponding to the hydrogen-desorption peak. $ECSA_{CO}$ can be calculated using the following equation:

$$ECSA_{CO} = (100\ Q_{CO}) / (Q_{CO(ref)}\ m) \quad (6)$$

In Eq. (6), Q_{CO} / µC is the charge calculated by integrating the area under CO desorption peak, $Q_{CO(ref)}$ is the charge needed for oxidation of the monolayer of adsorbed CO on the platinum surface, given as 420 µCcm^{-2}, and *m* is the mass of Pt loading (mg) indicating the amount of platinum on the working electrode. CO stripping gives realistic ECSA on Pt-alloys, whereas ESCA based on HUPD is usually lower [27].

Optimization approaches for PEMFC Cathode

Some approaches to optimizing Pt utilization in PEMFC cathode are described below:

Reducing Pt loading and decreasing Pt particle size

Typically, the performance of a catalyst layer (CL) has proportional relationship with the catalyst loading. However, in the case of platinum, there is a challenge of enhancing CL performance while decreasing Pt loading. In order to achieve this, reducing of particle size and improving Pt dispersion on the catalyst support have been explored. As was already reported, the effective particle size of Pt based catalyst is between 2 nm and 4 nm [28]. Since the percentage of exposed Pt decreases with increase of Pt particle size, only 20-50 % of total Pt is available for catalytic reaction, what is far below ideal dispersion.

Martin *et al.* [29] attempted to optimize electrode performance at significantly low Pt loading (0.012 mg cm^{-2}) obtained by electrospray method. By optimizing control parameters (Nafion® content, flow rate for electro-spraying catalyst ink and pressure for hot pressing MEA) they could achieve high

PtUt of 20 kW g^{-1} at 3.4 bar, a 70 °C. This is relatively high PtUt when compared to the previous of 3.3 kW g^{-1} [30]. Later on, the same team reported [31] further increase of PtUt to 30-35 kW g^{-1} at low Pt loading of 0.01 mg cm^{-2}, achieved by utilizing additional benefits of a microporous layer of carbon nanotubes coated on GDL as the cathode catalyst support. The authors also observed that Pt utilization remained unchanged for Nafion® content in the range of 30-50 %.

Wang *et al.* [32] fabricated MEA with low Pt loading of 0.022 mg cm^{-2} at the cathode side by simultaneously using electrospray and electrospinning (E/E) dispersion techniques, where they introduced Nafion® and Pt using two separate needles to produce Nafion® nanofibers and platinum nanoparticles (PtNP). Using this technique, they could regulate the size of fibers and loading of Pt catalyst, what resulted in improved ECSA with excellent Pt utilization of 42 kW g^{-1} for H_2/O_2 electrode at 0.022 mg cm^{-2} Pt cathode loading.

Alia *et al.* [33] developed a novel electrocatalyst using Pt/Pt alloy nanotubes (PtNT) and carried out voltammetry measurements for every 6000 cycles to investigate durability and ORR activity. They found that the electrode with cathode loading of 0.04 mg cm^{-2} showed highest ECSA of 23.9 m^2 g^{-1} with 127 % PtUt (Eq. 1) for which electrode porosity was stated as the reason.

Su *et al.* [34] combined ultrasonic spray coating technique and catalyst coated substrate (CCS) to achieve low Pt loaded gas diffusion electrodes (GDE). Four electrode samples with varying Pt loading (between 0.138 and 1.208 mg cm^{-2}) were studied at 160 °C (air and H_2 flow rate 250 and 100 cm^3 min^{-1}), while maintaining atmospheric conditions. As shown in Figure 3, they observed that current density values increased with decrease in Pt loading of cathode electrode and found that the electrode having 0.712 mg cm^{-2} Pt loading showed the highest current density values due to the highest ECSA. Therefore, low Pt loading electrode means thin CL, when most of the catalyst is concentrated in the interface between CL and electrolyte membrane, resulting in higher Pt utilization.

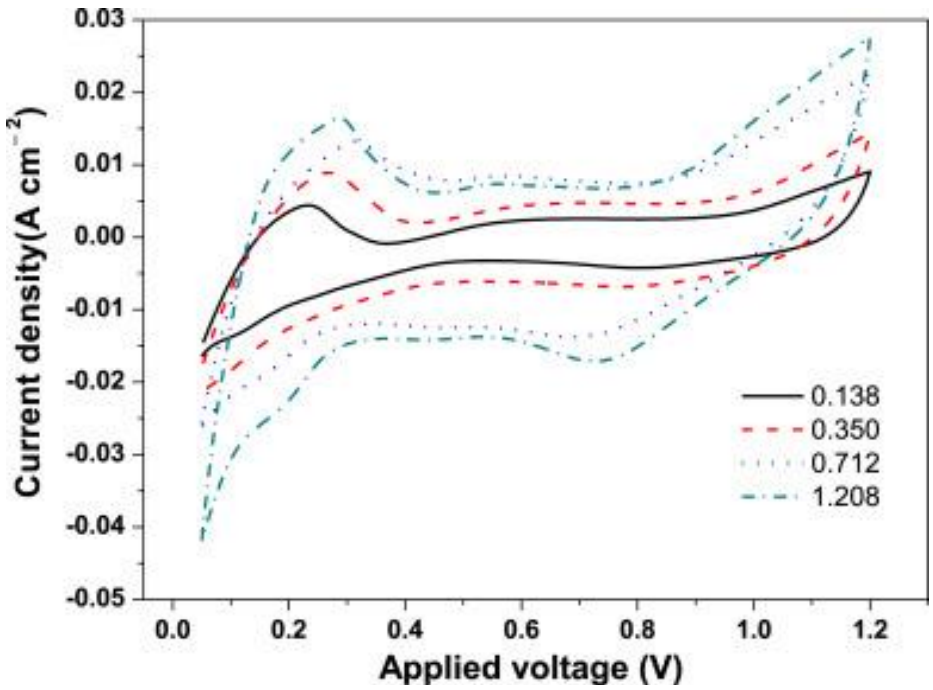

Figure 3. *CV profiles of GDEs with different catalyst loadings. Reproduced from [34] with permission from Elsevier*

Nabil *et al.* [35] electrochemically characterized the novel niobium carbide/carbon nano tubular porous structure (NbC) as the catalyst support for PEMFC electrodes. Supports were prepared by electrospinning and functionalized with Pt nano particles. The ORR activity and catalyst stability

(cc) BY

showed less ECSA for Pt/NbC/C (43 $m^2 g^{-1}$) than for geometrically calculated surface area (90 $m^2 g^{-1}$). The less conductive Nb_2O_5 was stated as a reason for lower PtUt. Also, 31 % retention in ECSA was observed for Pt/NbC/C after 10,000 cycles when compared with commercial Pt/C (only 5 % retention). The greater stability is attributed to the corrosion resistance of one dimensional NbC nanostructures.

The same group [36] using the same technique synthesized nanotubes with suitable properties as the catalyst support for PEMFC cathode. 3 mm Pt particles were deposited on NbC nanotubes. From electrochemical characterization, they observed less ECSA (43 $m^2 g^{-1}$) for 30 % Pt/NbC than for 50 % Pt/C. Also, better stability was found for the novel support than commercial 50 % Pt/C, when ECSA of both catalysts were equal. Summarized results for the above category are given in Table 2.

Table 2. *Reducing Pt loading and decreasing particle size (PEMFC cathode)*

Method / Technique / Support	Pt loading, mg cm^{-2}	ECSA, $m^2 g^{-1}$	PtUt, %	Reference
Electrospray	0.012	--		[29]
Carbon microporous layer (CMPL)	0.01	--		[31]
Electrospinning/Electrospray (E/E)	0.022	93.9		[32]
Porous PtNT	40	23.9	127	[33]
Ultra sonic spray coating technique	0.713	28.38	--	[34]
Electrospinning (Pt/Nb/C)	0.2	43	-	[35]
Electrospinning (Pt/Nb/C)	30 % Pt	43	-	[36]

Improving Pt dispersion

Dispersion of Pt on different carbon supports has been explored using various methods such as impregnation-reduction, ion exchange (IE), micro emulsion-based synthesis, *etc*. The supports used may include Vulcan, multiwalled carbon nanotubes (MWCNT), Vulcan XC-72R, carbon aerogel (CA), BP2000, activated carbon, carbon cryogel and others. The objective of dispersion is to reduce average Pt particle size and hence, to increase the catalytic surface area [37].

Bayrakceken et al. [38] deposited Pt nanoparticles of size 1-2 nm uniformly distributed on carbon supports (Pt/VXR, Pt/MWCNT, Pt/BP2000) using super critical carbon dioxide deposition technique (Figure 4).

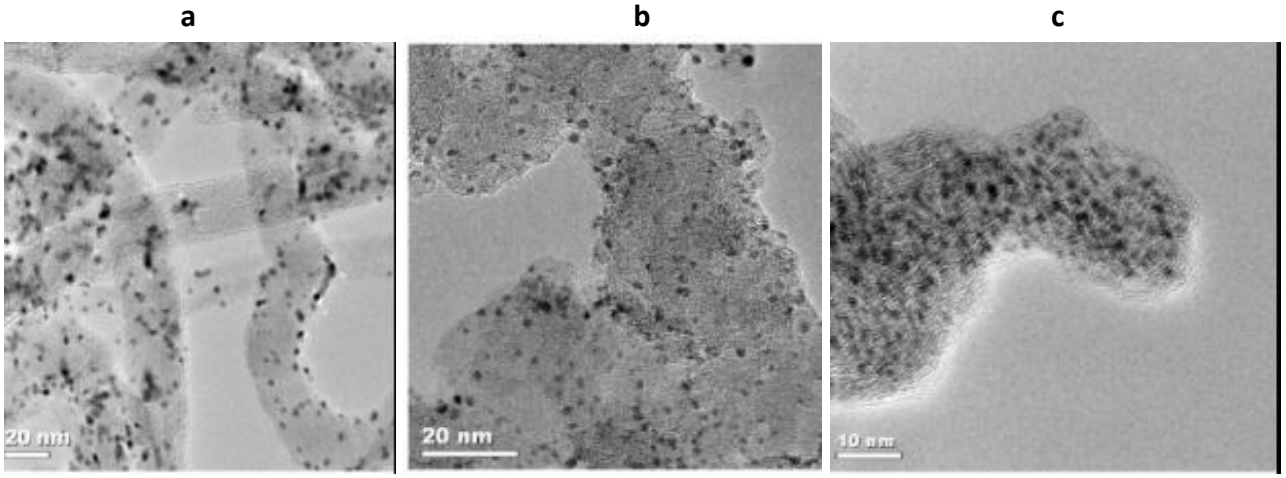

Figure 4. *HRTEM images of Pt particles on different carbon supports (a) Pt/VXR (b) Pt/MWCNT and (c) Pt/BP2000. Reproduced from [38] with permission from Elsevier*

They achieved nearly three times higher ECSA (173 $m^2 g^{-1}$ for Pt/VXR) with the reduced Pt loading when compared to a commercial catalyst (57 $m^2 g^{-1}$). The authors assumed that even for smaller Pt particles, the hydrophobic nature of carbon support makes Pt particles inaccessible for electrolytes.

Here, the highest PtUt of 93 % was observed for Pt/MWCNT with ECSA of 130 $m^2 g^{-1}$. The observed differences were due to variation in structure of carbon supports.

Fang *et al.* [39] deposited PtNTs on Vulcan XC-72 (VC) carbon black (CB) by employing the homogeneous deposition technique with ethylene glycol (EG) (reducing agent) using polyol process (HD-EG). They found higher ECSA of 78 $m^2 g^{-1}$ with high Pt utilization of 78 % when compared with the microwave (EG-MW) assisted polyol approach or conventional sodium borohydride ($NaBH_4$) reduction process. This highest Pt utilization (60 wt% on VC by HD-EG) was attributed to the relatively small PtNP with improved particle dispersion creating more active sites for the anticipated reactions.

Mroz *et al.* [40] used the pulse laser deposition (PLD) method for depositing catalyst films directly on Nafion® membranes and GDL and achieved accurately controlled low catalyst loadings with greater uniformity. Under various pressure ranges, electrodes were prepared and studied by varying thickness of the catalyst film between 0.09 and 3.47 nm, in proportion to the laser pulses between 75 and 3000. At low cell voltage, the results revealed higher current densities and less transport resistance of reagents when compared to cells with Pt catalyst placed on the Nafion® membrane. In the case of high cell voltages, low currents were generated due to less active surface area of Pt available for reactions. The authors stated that the efficiency can be further increased by growing the contact area between electrolyte and catalyst and also by enhancing the reaction zone to advance the passage of reagents.

Rost *et al.* [41] deposited Pt particles on carbon nanofibers (CNF) by employing the pulse plating technique (PPT). They observed 3.1 times higher ECSA of 148.6 $cm^2 mg^{-1}$ with CNF functionalization at 120 W for 10 min. The creation of the functional groups on fibrous surface of the nanoparticles and graphene (Gr) is stated as the reason for smaller and homogenous dispersion of catalyst.

Huang *et al.* [42] used the impregnation method to synthesize highly dispersed Pt catalyst with addition of centyltrimethylammonium bromide (CTAB) as dispersant at 300 °C. They prepared CL samples with different Pt loadings and observed higher ECSA and high PtUt for the catalyst sample with 4.12mg cm^{-2} dispersant concentration. The improved results were attributed to lypophilic alkyl and hydrophilic amine groups of CTAB.

Lv *et al.* [43] synthesized the novel carbon mixed carbide-based catalyst support (SiC/C) to improve electrochemical performance and catalytic activity of PEMFC cathode. They deposited Pt catalyst on nano SiC/C particles and observed homogenous dispersion of Pt particles on nano-SiC particles with evidently increased ECSA (48 $m^2 g^{-1}$) for Pt/SiC/C when compared to Pt/SiC (13 $m^2 g^{-1}$). The addition of carbon to Pt/SiC and uniform dispersion of Pt nano particles on the novel support were attributed to the increased PtUt in ORR activity of PEMFC electrode. Summarized results for the above category are given in Table 3.

Table 3. *Improving Pt dispersion (PEMFC cathode)*

Dispersion echnique dispersant	Catalyst support	Pt loading	ECSA, $m^2 g^{-1}$	PtUt, %	Ref.
$ScCO_2$	Pt/VXR	9.0 wt%	173	74	[38]
	Pt/CNT	9.9 wt%	130	93	
	Pt/BP2000	47.5 wt%	102	36	
HG-ED	CB	0.2 mg cm^{-2}	78	78	[39]
PLD	CB	1.24 µg cm^{-2}	-	-	[40]
PPT	Pt/CNF	1 mg cm^{-2}	148.6	-	[41]
CTAB	CTAB:	0.096 mg cm^{-2}	65.97	63.53	[42]
EG reduction method	Pt/SiC/C	20 %	48		[43]

(cc) BY

Structural modification of catalyst layer

Catalyst layer needs to be designed in order to ensure effective movement of electrons, protons, reactant gas, and water through a porous medium. Structural modification of CL aims to improve mass transport, decrease interfacial resistance between catalyst layer and gas diffusion layer, enhance catalyst utilization, and reduce Pt loading [44].

Su *et al.* [45] replaced the conventional double catalyst layer (DCL) with a novel double carbon layer (NDCL) cathode with high Pt content for inner layer and low Pt content for outer layer. Five cathodes (NDCL-1 to NDCL-5) with different Pt distribution ratio of inner and outer layers were prepared (Table 4).

From CV (Figure 5), better ECSA for the novel DCL than single catalyst layered (SCL) and conventional DCL catalysts can be observed. The highest ECSA of 81.4 $m^2 g^{-1}$ was recorded for NDCL-2 having the same inner and outer layer thicknesses, which was attributed to the reduced mass transport resistance. Further, the reduced catalyst and Nafion® content in outer layer was proved beneficial for ORR and water removal.

Table 4. *Five DCL cathodes with different inner and outer Pt distribution ratios [45]*

Novel double catalyst layer cathode	NDCL-1	NDCL-2	NDCL-3	NDCL-4	NDCL-5
Pt distribution (inner : outer)	9:1	8:2	7:3	6:4	5:5
L_{out}/L_{in} (estimated value)[a]	0.44	1	1.71	2.78	3.91

[a]L_{out}: outer catalyst layer thickness, L_{in}: inner catalyst layer thickness.

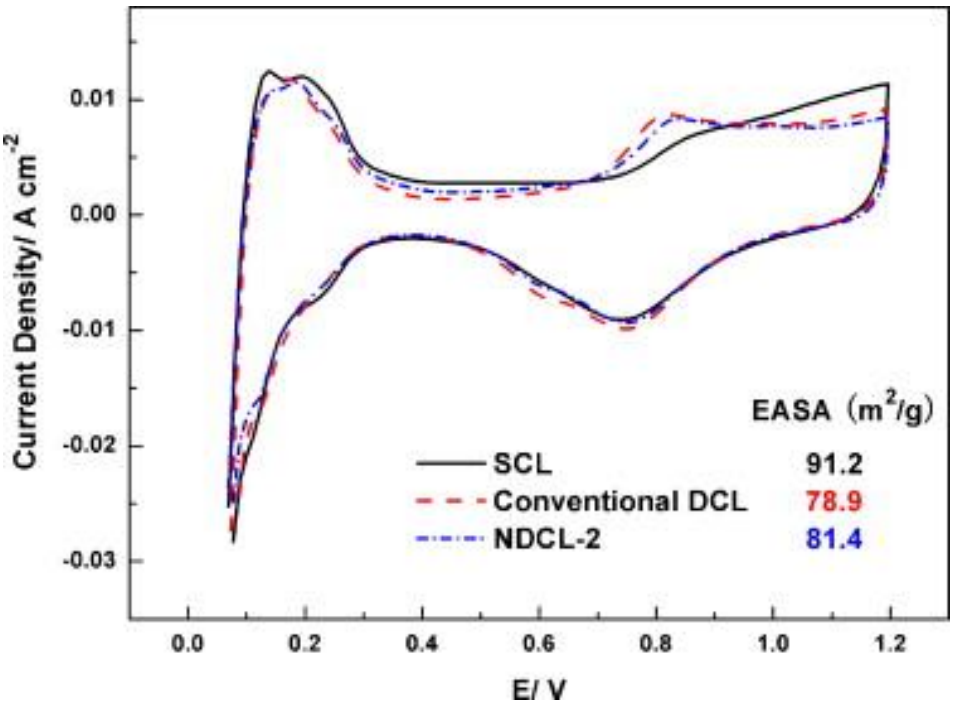

Figure 5. *CVs for MEA with single, conventional double and novel double catalyst layered cathode structures. Reproduced from [45] with permission from Elsevier (ESCA is marked as EASA on the graph*

Qiu *et al.* [46] developed a novel cathode structure (NCS) having double catalyst layer with reduced Pt loadings of 0.23 mg cm^{-2} and 0.11 mg cm^{-2} for inner and outer CL, respectively (Figure 6). The NCS was provided with hydrophobic and hydrophilic regions. It was observed that rich small pores of the outer layer provided efficient electrochemical active surface with the reduced GDL interfacial resistance, improving thus mass transfer. The compact structure of the inner layer

provided more active catalyst sites, resulting in improved migration of protons towards the membrane. The results showed 50 % Pt utilization for the developed NCS which was 28 % higher than that of traditional catalyst structure (TCS).

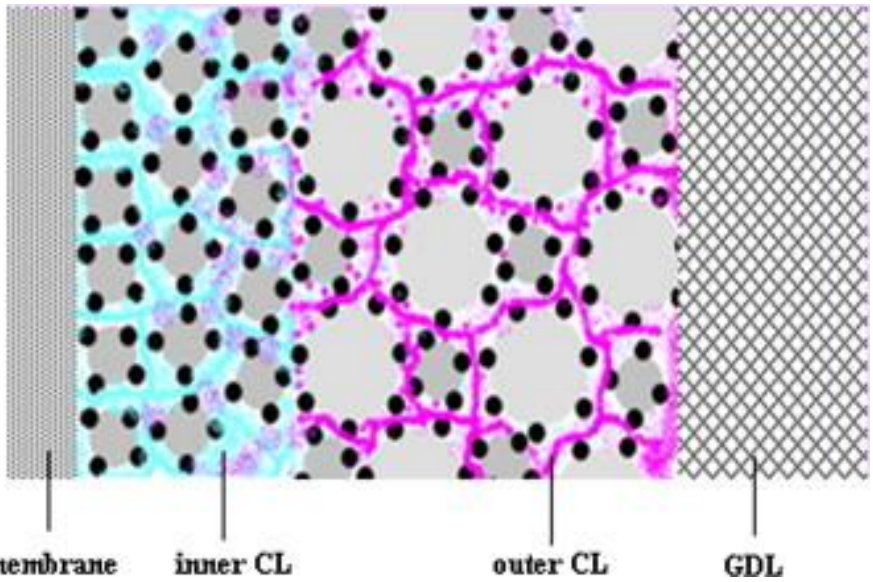

Figure 6. *Schematic of novel cathode structure (NCS). Reproduced from [46] with permission from Elsevier*

Avcioglu *et al.* [47] made an attempt to explain the significance of CL in water management since CL impacts water balance, while water flooding leads to mass transfer limitation at high current densities. To enhance durability performance and to ensure efficient thermal and water management in the components of PEMFC, the authors constructed a mesoporous hydrophobic channeled catalyst layer by addition of poly(tetraflouroethylene) (PTFE) nanoparticles and employing a two-step catalyst preparation method. By electrochemical characterization of three different types of catalyst *viz*., Pt/C, Pt/C-Nafion®, Pt/C-Nafion®/PTFE, it was found that addition of PTFE to the catalyst diminished Pt agglomeration, but reduced ECSA and PtUt of Pt/C-Nafion®/PTFE. It was concluded that higher ECSA (77 $m^2 g^{-1}$) was observed for Pt/C catalyst because of increased total catalyst surface area. The ECSA (70 $m^2 g^{-1}$) of Pt catalyst with Nafion® (Pt/Nafion®) was slightly reduced, but PtUt was improved due to formation of Pt agglomerates by Nafion® addition. The ECSA of Pt/Nafion®/PTFE, however, was only 45 $m^2 g^{-1}$ and PtUt was 56 % with enhanced diffusion process in the catalyst layer. Disruption of TPB, active sites blockage and increased average pore diameter were stated as the consequences of PTFE addition.

In order to overcome kinetic loss occurring at low Pt loading, Breitwieser *et al.* [48] employed a direct membrane deposition technique (DMD) in MEA fabrication process, wherein the conventionally free-standing membrane was replaced by two 8–15 µm thin ionomer layers with low Pt loading of 0.102mg cm^{-2} on anode and 0.029 mg cm^{-2} on cathode, respectively. At 300 kPa_{abs} of total pressure and under oxygen atmosphere, the DMD fuel cell yielded a maximum power density of 2.56 W cm^{-2} with very high PtUt of about 88 kW g^{-1}. This value was 2.3 fold higher than that of a commercial Nafion N-211 membrane reference fuel cell. The high PtUt efficiency was attributed to the novel DMD fabrication technique, which favored lower ionic resistance and improved power density in the high current density range.

To reduce Pt loading, Kaplan *et al.* [49] developed Pt alloys and core-shell structures. They synthesized two carbon supported Pt-surface enriched nano sized (Pt-SENS) catalysts and performed characteristic studies with a partial Pt shell and low-cost ruthenium (Ru) and iridium (Ir)

(cc) BY

metal cores. Instead Pt loading of 48 mg cm^{-2} for commercial Pt catalyst, they used Pt loading of 14 mg cm^{-2} for Pt/Ir/XC72 and 19.5 mg cm^{-2} for Pt/Ru/XC72 prepared electrodes. ECSA of 29 $m^2 g^{-1}$ was obtained for Pt/Ru/XC72 catalyst using CO-stripping method, while 26 $m^2 g^{-1}$ for Pt/Ir/XC72 and 48 $m^2 g^{-1}$ for 50 % wt Pt/C were obtained by HUPD method. It was concluded that Pt-surface-enriched structure increased availability of Pt particles for the catalytic reactions.

Chen *et al.* [50] designed a new gradient cathode with appropriate Pt/C ratio gradient direction (70 wt% inner side and 40 wt% outer sides) and Nafion® gradient span (33 wt% inner side and 23 wt% outer sides). This improved both Pt utilization and mass transfer, thus significantly improving the performance. Especially under low humidity, the performance of appropriate gradient MEA was 135.7 % higher than the MEA with SCL cathode at 20 % relative humidity. It also provided better water management, improved proton conductivity in cathode, and showed lower ohmic resistance and charge transfer resistance. Summarized results for the above category are given in Table 5.

Table 5. *Structural modification of catalyst layer (PEMFC Cathode).*

Novel Cathode Structure	Pt Loading	ECSA, $m^2 g^{-1}$	PtUt, %	References
NDCL	0.2mg cm^{-2}	81.4	--	[45]
NCS	0.4mg cm^{-2}	35.42	50.56	[46]
Pt/C	21 wt%	77	75	[47]
Pt/C-Nafion®	13 wt%	70	99	
Pt/C-PTFE	8 wt%	45	56	
DMD	29 µg cm^{-2}		88 kW g_{Pt}^{-1}	[48]
Pt/Ru/XC72	19.5 µg cm^{-2}	29	--	[49]
Pt/Ir/XC72	14 µg cm^{-2}	26	--	
Pt/C &Nafion® ratio	200 µg cm^{-2}	8.4	--	[50]

Optimization of catalyst parameters

High Pt utilization can be achieved by optimizing various catalyst layer parameters such as Nafion® content, Pt loading, Teflon content, catalyst layer and carbon support thicknesses, *etc.* [51].

Cheng *et al.* [52] investigated the effect of Nafion® and PTFE on PtUt for two catalyst layers: a) E-TEK electrode/GDE prepared using immersion method where Pt is impregnated with Nafion® and b) thin film catalyst layer (TFCL) prepared by blending Nafion® and Pt catalyst. PtUt of 77.8 % and 45.4 % were observed for the first and the second catalyst layer, respectively. It was concluded that while the catalyst particles are provided with sufficient passage ways for the transfer of protons in the first case, the thin film catalyst layer experienced lack of conduction because of the blockage of passage ways by the Nafion® solid.

Antolini *et al.* [53] investigated the effect of Nafion® loading on ORR at PEMFC electrode. They observed that the electrode exhibited poor electrolytic conductivity at low Nafion® loading and that ECSA increased with increasing content of Nafion® (Figure 7). The introduction of Nafion® is stated to improve the active surface area, resulting in better transport of protons through the electrolyte.

Sasikumar *et al.* [54] investigated the dependence of Nafion® content on Pt loading. Electrodes were prepared with different Pt loadings (0.5, 0.25, 0.1 mg cm^{-2}) and different Nafion® ionomer contents (20, 30, 40, 50, 60 wt%). The highest PtUt (52 %) was obtained at 40 wt% Nafion® content for Pt content of 0.25mg cm^{-2}. The authors concluded that Nafion® content must be determined by Pt loading and the fabrication technique used. The electrode performance was found to improve with enhancement of Nafion® content up to 40 %, but further increase in Nafion® content reduced the performance. The reasons attributed to this effect are blockage of Pt sites, decreased gas

permeability and augmented mass transport polarization. The increased distance for gas permeation, diffusion and migration are stated as reasons for transport limitation.

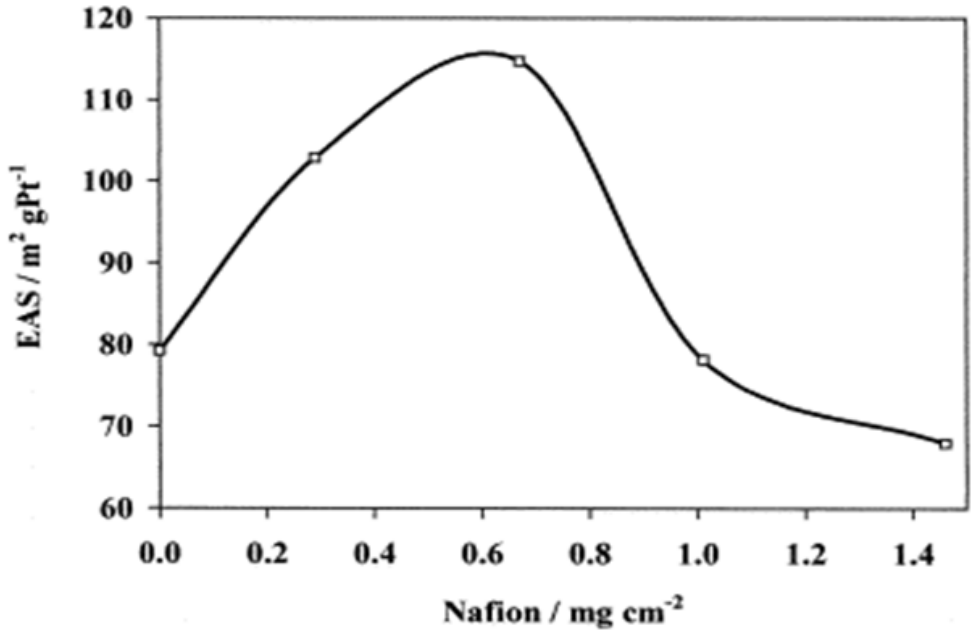

Figure 7. *ECSA (marked as ESA on the graph) variation with Nafion® loading in the CL (20* wt% *PTFE/C on DL, 0.2mg cm^{-2} of Pt in CL). Reproduced from [53] with permission from Elsevier*

Jiang *et al.* [55] studied the effect of thickness of carbon supported Pt catalyst layer in ORR using a thin film rotating disc electrode. Various catalyst layer thicknesses (0.25, 0.5, 1.0, 2.0, 4.0, 8.0 mm) were examined. The highest PtUt (77.9 %) was observed for 8.0 mm film. It was concluded that ECSA tends to increase with increasing thickness of the catalyst layer, showing more activity towards ORR accordingly.

Bayrakceken *et al.* [56] used super critical CO_2 deposition to prepare Vulcan supported Pt catalyst (Pt/Vulcan) and studied the effect of thermal reduction. Samples with Pt loading of 9 %, 15 %, 35 % were produced and ECSA were investigated using CV. The order of ECSA was found as follows: Pt/Vulcan 35 % < Pt/Vulcan 15 % < Pt/Vulcan 9 %. Although ECSA for Pt/Vulcan 15 % was found higher than for Pt/Vulcan 35 %, the PtUt was lower. This difference is, however, quite small (58 % *vs*. 62 %) and is not considered significant related to the uncertainty in both the calculated and the measured average Pt particle sizes. The difference in ECSA between Pt/Vulcan 15 % and 35 % catalysts is attributed to the differences in the Pt particle sizes, since ECSA Pt values differ by a factor of approximately 1.5.

Using plasma dc-magnetron sputtering technique, Khan *et al.* [57] studied the conical nanopillar structured Pt catalyst sputtered on the cathode with argon pressures of 0.05, 0.1, 0.5 mbar and at Pt loading range of 0.05 - 0.2 mg cm^{-2}. They observed high ECSA for the catalyst nanopillar deposited at 0.5 mbar at low Pt loading of 0.05 mg cm^{-2}. It was concluded that the deposition of uniform conical nanopillars on the electrode at high pressure improved catalytic activity and led to higher PtUt.

Slavcheva *et al.* [58] studied the effect of sputtering parameters (film thickness, argon pressure, dc-sputtering power) on thin films deposited by dc-sputtering technique. At low sputtering power (120–130 nm thick Pt films, 6 mTorr argon pressure, 100 W dc power), they found a stable and crystalline catalyst film with thickness between 120-130 nm, with large ECSA and PtUt. It was concluded that ECSA increased with increase of film thickness and improved the electrochemical activity towards ORR.

(cc) BY

Wang *et al.* [59] studied the influence of PTFE on electro spun/electro sprayed (E/E) MEA. They introduced only 1 wt% PTFE to the process which resulted in PtUt of 0.076 g kW^{-1} at only 0.094 mg cm^{-2} Pt loading. The improvement was attributed to enhanced hydrophobicity of the nanofibers which increases mass transfer and overall performance.

Speder *et al.* [60] studied the effect of Pt/carbon ratio on degradation of PEMFC catalyst. They used a colloidal synthesis approach for Pt/Vulcan and Pt/KetjenBlack catalysts using accelerated stress test (AST) in half cells. It was concluded that the loss in ECSA due to AST treatment depends on carbon support and Pt loading.

Zhao *et al.* [61] investigated the impact of pore size of FDU-15 (two-dimensional hexagonal ordered mesoporous carbon (OMC)) supported Pt catalyst by adopting a soft-template method. Samples with four different pore sizes ranging from 4.0 nm to 8.1 nm were prepared by the addition of pore expanding agents. By impregnation method, Pt catalysts were prepared using FDU-15 samples as catalyst supports and reducing agent, EG. CV and linear sweep voltammetry (LSV) measurements illustrated that catalyst with a pore size of 6.5 nm showed the highest ECSA (70.2 m^2 g^{-1}). It was also observed that Pt particle size is reduced with increase in pore size up to 6.5 nm and remained unchanged with further increase in pore size.

Kim *et al.* [62] examined the effect of diffusing solvents with varying main chain mobility of Nafion® to demonstrate large influence on Nafion® agglomerates, morphology and other properties such as proton conductivity and water uptake. The MEA synthesized from the dimethyl sulfoxide based isopropyl alcohol (IPA) and N-methyl-2-pyrrolidone (NMP)-based catalyst inks presented ECSA of 40.9, 43.0 and 52.5 $m^2 g^{-1}$, respectively. The introduction of diffusing solvents resulted in better diffusion of Nafion® into Pt/C aggregates, bringing more Pt particles in contact with Nafion® thereby increasing the catalytic activity at reduced current density.

Ruengkit *et al.* [63] investigated the influence of GDL properties (type of material (carbon paper (CP), carbon cloth (CC)), thickness, PTFE content and presence of micro porous layer (MPL)) on ECSA of Pt electrodeposited layer and fuel cell performance. Pt catalyst was electrodeposited by dc current onto GDL, with CC and CP of different thicknesses and hydrophobicity, and with and without presence of MPL. Despite their morphological differences, relatively similar ECSA (~120 $m^2 g^{-1}$ Pt) were obtained, while better performance for CC at higher current densities is due to its lower resistance and higher porosity. Pt deposited on a very thin GDL (90 µm) or GDL having high PTFE content (≥30 %) or containing MPL, consist of non-uniform particles distributed unevenly on the GDL surfaces, resulting in low ECSA (≤120 $m^2 g^{-1}$ Pt) and FC performances (i≤210 mA cm^{-2}). Pt electrodeposition on the CC having low PTFE content (10 %) produced small and uniform Pt particles distributed evenly throughout the GDL surfaces resulting in highest ECSA (193 $m^2 g^{-1}$ Pt). The same phenomenon was also observed for the two-layered GDL, which is attributed to the absence of the hydrophobic sublayer in the post-treatment of the GDL. It was concluded that selection of GDL as the fuel cell electrode is crucial when Pt catalyst is prepared by electrodeposition.

Egetenmeyer *et al.* [64] investigated electrodeposition of cathode catalyst layer using the plasma process. At different catalyst loadings and plasma durations, nanostructured Pt and Pt_3Co cathodes were prepared with varying quantity of ionomer and its distribution in the cathode catalyst layer (CCL). There was an increase of ECSA in comparison with the untreated substrate. ECSA increased with increase in the plasma treatment duration up to 23.1 $m^2 g^{-1}$ (highest) after 15 min plasma treatment, which is indicative of the deposition of smaller Pt particles on the electrode. Summarized results for the above category are given in Table 6.

Table 6. *Optimization of catalyst parameters (PEMFC cathode)*

Parameter/Variable/Method	Pt Loading, mg cm^{-2}	ECSA, $m^2 g^{-1}$	PtUt, %	Ref.
TFCL GDE	0.4	63.6 --	45.4 77.8	[52]
Nafion® loading	0.2	115	--	[53]
Optimum Nafion® content	0.25	648 cm^2	52	[54]
Thickness of CL	0.256	91.1	77.9	[55]
Thermal reduction($ScCO_2$)	0.028	173	74	[56]
dc-sputtering parameters	0.05	106.10	--	[57]
dc-magnetron sputtering parameters		47.09 cm^2	93.62	[58]
Effect of PTFE on electro spun /electro sprayed MEA	0.094	81		[59]
Platinum loading	14	126.5	-	[60]
Pore size on OMC/FDC-15	2	70.2	-	[61]
Solvent effect (NMP)	0.2	52.2	-	[62]
Effect of GDL thickness	0.25	193	-	[63]
Plasma process	0.3	23.1	-	[64]

Improving the performance of Pt support materials

The selection of appropriate support materials plays a key role in enhancing the overall performance of PEMFC and DMFC. Characteristics of good support material include presence of surface functional groups that promote catalyst-support interaction, mesoporous structure which improves triple phase boundary (TPB), good electrical conductivity and electrochemical stability, high surface area and corrosion resistance. Typically, conductive and porous membranes are known to possess above mentioned features and are therefore preferred as support materials for Pt catalyst [44].

Existing research reveals that use of carbon-based support with various structural and morphological properties improved stability and electrocatalytic activity of catalyst. In addition, mass transfer and electronic conductivity in CL are also found to be enhanced at carbon supports. Some of the novel carbon-based support materials investigated so far are carbon nanofibers (CNF), ordered mesoporous carbons, carbon aerogels, carbon nanohorns, carbon nanocoils and carbon nanotubes (CNT) [44].

In this connection, Zhao *et al.* [65] demonstrated that nearly 100 % of Pt can be exposed to catalytic activity by using gold nanoparticles as Pt catalyst support (AuPt). ECSA measurements were carried out on Vulcan XC-72 CB samples by varying Pt and Au ratio. Prominent enhancement of ECSA and Pt utilization was observed when Pt/Au ratio becomes lower than 0.2. Further decrease of Pt/Au ratio to 0.05 or less, makes ECSA and PtUt to increase up to 100 %. This approach ensured uniform dispersion of Pt particles and prevented pocketing in the micropores of supported material, making thus Pt particles efficient for ORR.

Kongkanand *et al.* [66] and Orfanidi *et al.* [67] elucidated use of carbon nanotubes (SWCNT) and (MWCNT) as Pt catalyst supports. Pt particles supported on SWCNT showed lower ECSA (17.8 $m^2 g^{-1}$) than the commercial carbon support (33.5 $m^2 g^{-1}$) with 10 mV shift in the onset potential for ORR. They inferred that the commercially available Pt has better distribution of Pt nanoparticles than the one developed in the lab with SWCNT. Pt supported on MWCNT, however, showed improved ECSA of 78.4 $m^2 g^{-1}$ with 84 % PtUt. Higher ECSA and better catalytic utilization were attributed to uniform dispersion and narrow particle size distribution (2.5 to 4 nm).

Instead of using pure SWCNT, Zhu *et al.* [68] used a mixture of SWCNT and carbon nanofibers (CNF) at 1:3 (SF13) and 1:5 (SF15) ratios (Bucky paper) to prepare a novel catalyst. They observed reduced ECSA due to larger Pt particle size (6 nm) than of commercial catalyst support (2 nm). However, PtUt

(cc) BY

of 88 % and 84 % for SF13, SF15 were observed which was ascribed to availability of the catalyst particles at electrolytic and electronic pathways of the Bucky paper electrodes.

Kou *et al.* [69] investigated the properties of functionalized graphene sheets (FGS) as the cathode catalyst support, mostly because of higher conductivity, high surface area and low manufacturing cost with unique graphitized basal plane structure. Results revealed higher initial ECSA (109 $m^2 g^{-1}$) with improved stability when compared to the commercial catalyst (E-TEK, 75 $m^2 g^{-1}$). This was attributed to smaller Pt particle size of 2 nm and less extent of Pt nanoparticles agglomeration on FGS.

Salernitano *et al.* [70] used the controlled plasma improved chemical vapour deposition (CVD) technique to deposit Pt nanofibers on a support made from carbon nano fibers (CNF). Electrodes were prepared with different structures of CNF, by changing the orientation of graphene layers in relation to the fiber axis. This resulted in availability of large number of active sites for catalyst nanoparticles. Due to the controlled morphology grown of graphite paper, they found higher ECSA (225 $m^2 g^{-1}$) with improved PtUt at reduced Pt loading (0.018 mg cm^{-2}).

Huang *et al.* [71] used conductive titanium oxide as Pt catalyst support and investigated Pt/TiO_2 durability and stability using in-house potential cyclic experiments. Although initially, the Pt/TiO_2 (31.2 $m^2 g^{-1}$) showed less ECSA than Pt/C (56.4 $m^2 g^{-1}$), it continued to remain stable even after 4000 cycles with minimum loss in ECSA. On the contrary, Pt/C showed no activity after 2000 potential cycles owing to Pt dissolution, carbon corrosion and Pt particles sintering. ECSA was calculated after 2500 cycles and observed larger ECSA for Pt/TiO_2 than Pt/C catalyst.

Song *et al.* [72] developed the novel compound carbon supported Pt catalyst (Pt/CCS) by introducing ultra-fine porous carbon fibre (UPCF) powder to commercial Pt catalyst as a second carbon support. Partially supported Pt catalyst JM-40 catalyst with particle size 3.4 nm was combined with UPCF. Using CV measurements, it was observed that Pt/CCS-20 showed the highest PtUt with ECSA 71.9 $m^2 g^{-1}$.

Sanli *et al.* [73] used reduced graphene oxide (rGO) and carbon black hybrid material as Pt support and fabricated a novel cathode structure for PEMFC. Using electrospray technique, they synthesized platinum/reduced graphene oxide (Pt/r-GO) electrocatalyst and platinum/reduced graphene oxide/Vulcan XC-72, Pt/r-GO/VXC-72, hybrid electrocatalyst with 50 wt% r-GO. Comparing the results with air-sprayed electrode, it was observed that Pt supported on the hybrid support (Pt/r-GO/Vulcan XC-72) showed higher PtUt efficiency with relatively low Pt loading. This enhancement of the electro-sprayed hybrid electrode was credited to facile proton and oxygen transport to the catalytic sites, what resulted from electrode morphology and hybrid support structure. Thus, efficient diffusion of reactant gases to the catalytic sites was achieved.

Singh *et al.* [74] used carbon aerogel which was synthesized by impregnating Pt nano particles using the microwave assisted polyol process. Performance and stability were investigated, and results compared with those for commercially available Pt/C (JM-20) having the same Pt loading. ECSA of 73 and 56 $m^2 g^{-1}$ for Pt/CA and commercial JM-20, respectively were obtained. It was concluded that good utilization ratio of 82 % could be due to the conducting and mesoporous CA support which has significant role in improving Pt activity and Pt utilization.

Lori *et al.* [75] employed the modified polymer-assisted deposition (mPAD) technique and synthesized molybdenum carbide (Mo_2C) nano-crystallites without free carbon and used them as the catalyst support, showing ECSA of 28.4 $m^2 g^{-1}$. The reason for low ECSA was attributed to formation of aggregates during deposition, making Pt particles inaccessible for reactions.

Ignaszak *et al.* [76] studied titanium carbide (TiC) and core shelled TiC@TiO_2 material as catalyst supports for Pt and Pt_3Pd alloy (Pt/TiC, Pt_3Pd/TiC, Pt_3Pd/TiC@TiO_2) for ORR activities. They observed

close values of ECSA (40, 41 and 37 $m^2 g^{-1}$) for all three catalysts with no significant difference in electrochemical features. However, $Pt_3Pd/TiC@TiO_2$ retained its activity after 500 cycles, while significant loss of activity was noticed for Pt/TiC and Pt_3Pd/TiC.

To overcome the drawbacks of carbon supports of PEMFC electrodes, Lobato *et al.* [77] prepared MEAs with two non-carbonaceous catalyst supports, SiC and SiCTiC, for PEMFC cathode side and compared the electrochemical performance with carbonaceous support. They observed that catalyst supported on novel materials (Pt/SiC, Pt/SiCTiC) showed excellent electrochemical stability towards environmental corrosion, what was attributed to higher catalyst particle size. Also, at the end of 400 cycles, less ECSA degradation of 19.7 % for Pt/SiC and 17.01 for Pt/SiCTiC was observed when compared to commercial (31.09 %) and homemade (29.82 %) catalysts.

In an effort to find better alternative to carbon support for PEMFC catalyst, Shahgaldi *et al.* [78] synthesized a novel nano composite, titanium encapsulated in carbon nanosperes and carbon titanium core shell structures as cathode catalyst supports, using simple and less costly hydrothermal method. They prepared 10 % and 20 % TiO_2 encapsulated carbon (EC-10, EC-20) and core shell structures (CS-10, CS-20). The electrochemical study revealed that 10 % TiO_2 samples (EC-10, CS-10) showed higher ECSA (414 and 440 $m^2 g^{-1}$) than EC-20, CS-20 (280 and 180 $m^2 g^{-1}$), suggesting the effect of TiO_2 amount on the active surface area.

Using a new synthesis method, Borchardt *et al.* [79] prepared Pt metal containing silicon carbide derived carbon (CDC-Pt). They reported high ECSA (66 $m^2 g^{-1}$) for the synthesized catalyst than conventional Pt/C catalyst and concluded that the deposition of Pt nanoparticle onto carbon matrix provided long term stability with superior corrosion stability. Summarized results for the above category are given in Table 7.

Table 7. *Carbonaceous and non-carbonaceous electrocatalysts support materials (PEMFC cathode)*

Catalyst support	Pt Loading,mg cm^{-2}	ECSA, $m^2 g^{-1}$	PtUt, %	Ref.
Gold Nanoparticles(AuPts)	0.012	234.1	99.5	[65]
Single Wall Carbon Nanotubes(SWCNT)	0.014	17.8	--	[66]
Multiwalled Carbon Nanotubes(MWCNT)	0.005	78.4	84	[67]
Buckypaper	0.09, 0.14	43.3, 39.2	88, 84	[68]
Functionalized graphene sheets(FGS)	20 wt%	109	--	[69]
CarbonNanoFibers (CNF)	0.3	225	--	[70]
Titanium oxide	0.4	31.2	--	[71]
Ultra Porous Carbon Fiber (UPCF)	0.35	71.9	87.2	[72]
Pt/rGO/CB (H75) (hybrid support)	0.5	102		[73]
Carbon Aerogel(Pt/CA)	0.4	73	-	[74]
Molybdenum Carbide(Pt/Mo_2C)	0.096	28.4	-	[75]
TiC, $TiC@TiO_2$(Pt-TiC, Pt_3Pd-TiC-TiO_2)	0.048	40, 36	-	[76]
SiC, SiCTiC (Pt/Sic, Pt/SiCTiC)	0.6	13.36, 13.20		[77]
TiO_2, C-TiO_2 (Pt/TiO_2,Pt/C-TiO_2)	0.1	414, 440		[78]
Si –CDC (Silicon carbide derived carbon)	12 wt%	66		[79]

Developing Pt metallic alloy and Pt-free catalysts

Pt metal is alloyed with other elements to decrease the overall cost of electrodes. Several studies have been performed to obtain nearly equivalent or better catalytic activity through the introduction of Pt based binary systems such as Pt-Ni, Pt-Fe, and Pt-Co by varying the proportion of Pt and the alloying metal. In addition, the performance of some Pt free catalysts has also been explored [80,81].

(cc) BY

Using simple chemical reduction method, Wu *et al.* [82] prepared 20 wt% Pt and nickel (Ni) catalyst with XC-72 conducting furnace black (PtNi/XC-72) and graphene (PtNi/graphene) as carbon supports. From results of chemical characterization, they found that ECSA of catalyst samples are in the following order: Pt/XC-72 < PtNi/graphene < PtNi/XC-72.

Owing to their special electrical properties, PtNi/XC-72 and PtNi/graphene electrodes showed better catalytic activity towards oxygen reduction when compared with Pt/XC-72. PtNi/graphene showed better performance than PtNi/XC-72. Due to enhanced catalyst carbon interaction and high graphite component, graphene has the potential to provide much higher durability than XC-72.

Sahoo *et al.* [83] synthesized doped porous carbon (DPC) with nitrogen and sulphur in a simple and green one-pot process from ionic liquid as the sole source precursor and used as the non-Pt cathode catalyst in PEMFC. The results of half-cell and full cell studies were compared with Pt decorated DPC (Pt/DPC). The ECSA for Pt/DPC and commercial Pt/C after ignoring the role of electric double layer formed between electrode and electrolyte, were 46.88 and 112.34 $m^2 g^{-1}$ with Pt utilization efficiency 98.2 % and 60.2 %, respectively. The even distribution of Pt nanoparticles over high surface area and porous support of doped carbon material is stated as a reason for 2.5 times higher ECSA for Pt/DPC when compared to commercial Pt/C.

Wang *et al.* [84] synthesized a variety of Pt–Ni alloy catalysts by potentiostatic electrodeposition. They use an orthogonal array to optimize deposition parameters. Particularly, the electrochemical performance of Pt–Ni alloy catalysts was optimized by dealloying treatment experiment conducted at 0.35 V, 20 min at 50 °C. The results indicated that the deposition time has the most significant impact on the performance of Pt–Ni alloy catalysts. The prepared sample (Pt-Ni) showed the highest ECSA value of 81.7 $m^2 g^{-1}$ with the catalyst loading of 0.329 mg cm^{-2} (Pt loading of 0.3 mg cm^{-2}, Ni loading of 0.029 mg cm^{-2}). Pt–Ni catalysts were dealloyed by rapid potential cycling, which resulted in a significant refinement of morphology and enhancement of electrocatalytic activity. The sample with low Ni atomic ratio was not suitable for the rapid dealloying treatment.

Pt–Cu (platinum copper alloy) has been studied as a catalytically active material with high surface area, porous platinum structure and hydrogenation promoting property [85].

Bele *et al.* [86] demonstrated the application of stable and highly active $PtCu_3$ nanoparticles on the carbon support. The Pt-skin $PtCu_3$ alloy catalyst was fabricated with core shell nanoparticles having intermetallic ordered shell at a disordered core that is tightly embedded into a carbon support. Consistent ECSA of about 45 $m^2 g^{-1}$ is reported with utilization much higher than those already reported in the literature for 3 nm Pt nanoparticles on high surface area carbon supported electrodes. The thermal annealing enables Pt-skin and intermetallic orderings, which are favorable for enhanced activity. The stability is attributed to the firm embedding of Pt-Cu into a heterogeneous carbon matrix caused by the partial oxidation and xerogelation.

Mani *et al.* [87] proposed the technique of surface dealloying as an effective strategy to modify the surface electrocatalaytic properties of platinum. The copper (Cu) surface atoms are dealloyed from $Pt_{25}Cu_{75}$ alloy precursor compound by electrochemical dissolution (voltammetric dealloying to prepare the active catalyst phase). This novel catalyst yielded an ECSA of 75 $m^2 g^{-1}$.

Hong *et al.* [88] fabricated a novel electrode, Pd/C@Pt_{skin} (C-U), with electrospun structure by using electrospinning and under potential deposition (UPD) techniques. By in situ deposition of Pt on the surface of Pd-NP in the electrospun Pd/C catalyst layer, they observed that almost all Pt shells become accessible for reactant gases and TPB is optimized with Pt loading of 19 mg cm^{-2}. The C-U electrode delivered higher peak power density (0.62 W cm^{-2}) than conventional electrode (0.55 W cm^{-2}) at Pt loading of 100 mg cm^{-2}. Owing to the nearly 5-fold Pt loading, the conventional electrode showed

better performance than C-U electrode at low current density, however at high current density there was a significant loss of voltage. This was due to the increased oxygen transfer resistance close to Pt surface. Summarized results for the above category are given in Table 8.

Table 8. *Developing Pt metallic alloy and Pt-free catalysts*

Pt metallic alloy & Pt free metal	Pt loading, mg cm^{-2}	ECSA, $m^2 g^{-1}$	PtUt, %	References
PtNi/XC-72	0.2	93	-	[82]
Pt/DPC	0.2	112	98	[83]
Pt- Ni alloy	0.3	81	-	[84]
$Pt\text{-}CU_3$	0.025	45	-	[86]
$Pt_{25}Cu_{75}$	0.169	75	-	[87]
C-U electrode	330	92.3	-	[88]

Optimization approaches for DMFC cathode

Some approaches for optimizing Pt utilization in DMFC cathode are described below.

Reducing Pt loading and decreasing Pt particle size

Wang *et al.* [89] observed that addition of NaOH to aqueous Nafion® solution suppressed aggregation of large particles and led to smaller agglomerate particle size with uniform distribution of Pt elements in the cathode catalyst layer. Further, they obtained improved ECSA (13.94 $m^2 g^{-1}$) and better performance in DMFC.

To enhance Pt utilization, You *et al.* [90] adopted multi step reduction, Pt/C-nR (n = number of reduction steps), to synthesize Pt catalyst with ultra-high Pt loading up to 85 %. CV results revealed that Pt/C-2R catalyst exhibited higher PtUt of 90 % when compared to Pt/C-1R (60 %) with the same Pt loading. Although Pt particles size appears to be larger for Pt/C-1R than Pt/C-nR, the stacked microstructure in Pt/C-1R is stated to favor higher PtUt.

Wang *et al.* [91] investigated electrochemical oxidation of methanol and reduction of oxygen on the commercial Pt/C catalyst. High catalytic current was observed for ORR with ECSA of 41 $m^2 g^{-1}$.

To improve DMFC performance, Pu *et al.* [92] utilized fabricated Pt nanorod assemblies in double layered cathode with a catalyst loading of 1.0 and 2.0 mg cm^{-2} and observed significant increase in ECSA (35.5 $m^2 g^{-1}$) and catalyst utilization. The improvement in performance is attributed to the reduction of charge transfer resistance in DMFC, enabling more efficient Pt loading and improving performance of MEA. The increased ECSA is attributed to the reduced size of Pt particles, loose construction of Pt nanorods and embedding of nanorods in the catalyst layer.

Optimization of catalyst parameters

Krishnamurthy *et al.* [93] **s**tudied the performance of DMFC by varying the content of Nafion® in anode CL while keeping it constant on cathode. The optimized results showed the highest catalyst utilization of 65 % at 0.8 Nafion® to carbon (N/C) ratio. Further increase of Nafion® content was reported to result in pore blocking of the catalyst layer which leads to decrease in performance of DMFC.

Krishnamurthy *et al.* [94] studied the influence of PTFE content of anode and cathode CLs on DMFC performance. They examined 5, 10, 20, 30 % PTFE content in cathode CL with anode having constant PTFE content of 20 %. They observed the highest catalyst utilization of 65.54 % for 20 % PTFE and concluded that 20 % PTFE content in the cathode catalyst layer resulted in the maximal catalyst utilization. They also concluded that further increase in PTFE content to 30 % leads to the

(cc) BY

blocking of pores of CL, thus reducing oxygen transportation and water removal. The same authors [95] also studied the catalyst utilization by varying Nafion® content. 20 % Pt/C, 40 % Pt/C and platinum black were used as cathode catalysts and the Nafion® content was optimized for each. Based on CV results, the highest value of catalyst utilization of 65 % for 33 % constant Nafion® content with 40 % Pt/C catalyst layer was obtained. No significant influence of Nafion® content on platinum black catalyst was also observed.

Matar *et al.* [96] investigated the effect of thickness of cathode catalyst on DMFC performance. They considered 8.4 µm thickness layers as standard/base thickness for both anode and cathode with same Pt loadings. Two additional cathode catalyst layers with 19 and 44 µm were examined. The authors observed decrease of ECSA as thickness of cathode catalyst layer increased and found higher ECSA of 282.88 $cm^2\ mg^{-1}$ for the standard/base case (8.4 µm).

Using citrate stabilized method, Jiang *et al.* [97] prepared 60 % Pt/C catalyst by varying carbon supports and reductants (Pt/XC-72, Pt/BP2000, Pt/XC-72R). They observed that Pt/BP2000 support resulted in higher ECSA (66.46 $m^2\ g^{-1}$) with improved catalyst utilization. The difference in performance was attributed to the addition of chloroplatinic acid solution to citrate which contributed to formation of small Pt particles corresponding to large specific surface area with high ECSA and catalytic activity.

Moore *et al.* [98] investigated catalytic activity of DMFC in terms of morphology of porous cathode catalyst substrate. They synthesized three electrocatalysts, *i.e.* Pt/C-Celatum (a macro porous carbon substrate), Pt/CMK-3 (a mesoporous carbon substrate), and Pt/Vulcan XC-72 (a micro porous carbon substrate). After CV studies, they observed major variation between active surface area and total surface area for Nafion® impregnated sample (Pt/C-Celatum). It was concluded that the difference is due to reduced contact between Nafion® electrolyte and catalyst surface, blockage of the pores, and poor accessibility of protons between crystalline platinum and carbon substrate, which all led to low Pt utilization.

Zhao *et al.* [99] employed an electrochemical technique to investigate the influence of Nafion® ionomer content (10, 20, 30, 40, and 50 wt%) catalyst layers on the cathode performance. They found the highest ECSA (27 $m^2\ g^{-1}$) and catalyst utilization (40 %) at 30 wt% Nafion® content with less difference between the highest and lowest ECSA and concluded that Nafion® content has less effect on ECSA and PtUt in 10-50 wt% range. Figure 8 illustrates the effect of Nafion® content on ECSA and Pt catalyst utilization.

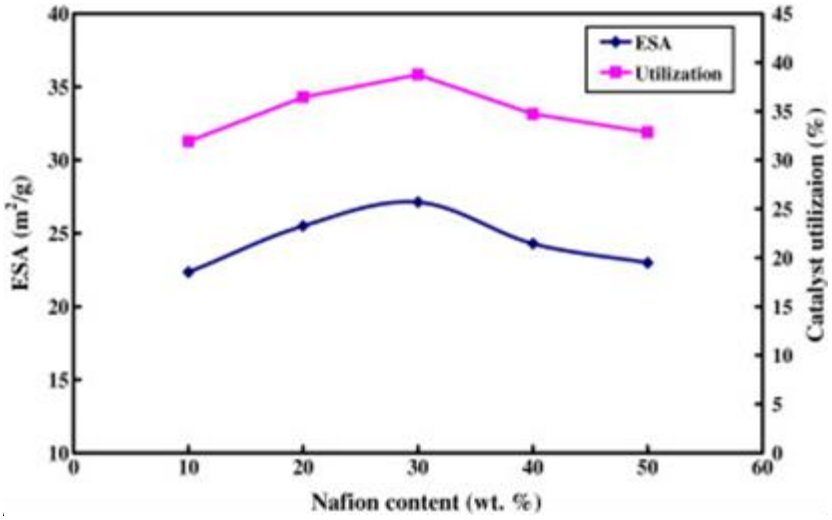

Figure 8. *Effect of Nafion® content on Pt utilization and ECSA (marked as ESA on the graph). Reproduced from [99] with permission from Elsevier*

Using various novel catalyst support materials

Wang *et al.* [100] fabricated DMFC cathode using high surface area SWCNT (Pt/SWCNT) to increase the triple phase boundary sites. Pt/SWCNT was prepared using ion exchange (IE) method and the performance with borohydride (BH) synthesis method was compared. They observed improved Pt utilization and concluded that entire catalyst particles were loaded on SWCNT support, being well dispersed (by IE method) and electrochemically active.

Chen *et al.* [101] used microwave digestion modified carbon nanotubes (CNT) on CC as the catalyst support. Larger ECSA than the others were found, which is attributed to higher Pt dispersion and uniform distribution of Pt nanoparticles.

Yaldagard *et al.* [102] studied the performance of Pt electrocatalyst supported on the protonated polyaniline (PANI) coated tungsten carbide (WC) nano composite and compared the results with the commercial Pt/C electrocatalyst. High Pt utilization of 77 % compared to the commercial one was found, and this improvement was attributed to the synergic effect between Pt nanoparticles and WC.

Jafri *et al.* [103] synthesized nitrogen doped graphene to support Pt catalyst. They used MWCNT spacer to remove face to face agglomeration, what cleaned graphene sheets. Two types of samples, Pt/NGA800+MWCNT, Pt/NG180+MWCNT, were prepared using thermal solid state and hydrothermal methods and compared the results with samples without MWCNT spacer (Pt/NGA800, Pt/NG180). The authors observed 10 % improvement in ECSA and 55 and 54 % Pt utilization and concluded that the addition of MWCNT spacer provided good accessibility to the catalyst active site and nitrogen doped CNT, what resulted in decomposition of reactive intermediates like H_2O_2 into O_2 during ORR.

Algere *et al.* [104] investigated sulfurized carbon xerogels (S-CXG) as the support material for Pt. The highest catalytic activity was observed for Pt/CXG-3S (3 wt% sulphur content) because of right balance of high ECSA (59.0 $m^2 g^{-1}$) and good intrinsic activity. It was found that Pt/CXG-3S exhibited better catalytic activity than Pt/CXG without sulfurization or Vulcan.

Tesfu *et al.* [105] investigated the use of mesoporous structured hollow graphitized carbon spheres (HGS) as DMFC cathode catalyst support material in 100-150 °C temperature range. Pt/HGS catalyst showed improved ECSA and double layer capacity values which is attributed to higher accessibility of Pt particles. However, large decrease in ECSA (60 % compared to 14 % for Pt/Vulcan) was observed at thermal treatment beyond 850 °C. They inferred that this does not correlate with increased particle size and concluded that during thermal treatment, the decomposition of HGS carbon structure resulted in the blockage of pores, making Pt active sites inaccessible to the electrolyte.

Developing Pt metallic alloy and Pt-free catalysts

Hosseini *et al.* [106] synthesized Ni/Pt/C electrocatalyst using sodium borohydride as the reducing agent and sodium dodecyl sulphate (SDS) as a structure directing agent. This electrode exhibited improved catalytic activity than NiPt/C catalyst. ECSA of 41 % (Ni/Pt/C) and 16.8 $m^2 g^{-1}$ (NiPt/C), respectively, were recorded. Core shell structure of the prepared catalyst was stated as the reason for the increased ECSA and current density. Summarized results for the above category are given in Table 9.

(cc) BY

Table 9. *Platinum utilization for DMFC cathode*

GDE/structure/support/membrane/ parameters	Pt loading, mg cm^{-2}	ECSA, $m^2 g^{-1}$	PtUt, %	Ref.
Reducing platinum loading and decreasing Pt size				
Effect of Nafion® ionomer aggregation	6.3	13.94		[89]
Multi Reduction method Pt(76)/C-1R /Pt(76)/C-2R	2.0	60.2 /65.3	68 / 90	[90]
PtNT	-	41	-	[91]
Double layered catalyst based MEA	1.0, 2.0	35.5, 34.3		[92]
Optimization of catalyst parameters				
Nafion® to carbon (N/C) ratio	2.0	-	6	[93]
Effect of Polytetrafluoroethylene(PTFE)	2.0	57.0	65.54	[94]
Effect of Nafion® content	40 wt%	67.03	65.12	[95]
Cathode catalyst layer thickness	1	28.3	-	[96]
Citrate-stabilized method with different reductants and carbon supports (Pt/BP2000)	2.8	66.46	-	[97]
Effect of the cathode catalyst substrate morphology (Pt/Vulcan XC-72)	1	33.4	25.1 %	[98]
Influence of ionomer content(30 % Nafion®)	2	28	40 %	[99]
Using various novel catalyst support materials				
Pt/SWCNT	11.8 wt%	129.6 cm^2	90 %	[100]
Pt/MWCNT	0.3	23.9 cm^2	25.1 %	[101]
Pt/PANI/WC/C	4	20.46	77 %	[102]
Nitrogen doped graphene with MWCNT spacer (Pt/NG1800+MWCNT)	0.42	47	55 %	[103]
Carbon Xerogels (CXG)	20 wt%	59.0	-	[104]
HGS	2			[105]

Optimization approaches for DMFC anode

Some approaches to optimizing Pt utilization in DMFC anode are given below.

Optimization of catalyst parameters

Liang *et al.* [107] electrochemically deposited Pt nanowires into partial layer of nano Nafion® membrane and formed Pt nanowire network. CV tests showed large ECSA for Pt Nafion® integrated electrodes than conventional E-TEK electrode. Initial results revealed higher ECSA for Pt-Nafion® integrated electrode and a low rate of methanol. Utilization of methanol during the discharge of cell and increased membrane tortuosity are attributed as reasons for enhancement of the catalytic activity.

Scibioh *et al.* [108] explored the ionomer coating (1, 2, 5 wt%) on Ketjen Black EC 300JD (EC), Vulcan XC-72R (VC) and Black Pearls 2000C (BP) carbon supports with different surface area and pore characteristics. They observed better performance for EC5 (Ketjen Black EC 300JD coated with 5 wt% Nafion®) due to extension of TPB, resulting from the improved interaction between catalyst particles and ionomer.

Pu *et al.* [109] employed a thermal imprint technology to prepare passive DMFC using Nafion® 115 membrane on the anode side. The anode catalyst utilization was found to be improved with improved ECSA, which is credited to the additionally increased roughness factor of membrane. They concluded that catalyst utilization at the anode can be improved by using patterned membranes H_4, H_6, H_{10}, with pore depths of 4, 6, 10 µm and roughness factors 2.7, 4.6, 5.4 and observed the highest ECSA for H_{10} membrane.

Kaplan *et al.* [110] studied platinum utilization on methanol-oxidation surface by varying Pt:Ru surface composition. Carbon-supported catalysts with iridium-nickel cores and varying atomic-ratio platinum ruthenium shells ($Pt_{25}Ru_{75}$ to $Pt_{80}Ru_{20}$) were synthesized. The ECSA values obtained for the studied catalysts were 50 $m^2 g_{PtRu}^{-1}$ for the commercial catalyst, 35 $m^2 g_{PtRuIr}^{-1}$ for $Pt_{13}Ru_{22}$, 28 $m^2 g_{PtRuIr}^{-1}$

for $Pt_{16}Ru_{14}$, 27 $m^2\ g_{PtRuIr}^{-1}$ for $Pt_{23}Ru_9$, and 27 $m^2\ g_{PtRuIr}^{-1}$ for $Pt_{28}Ru_7$. The highest mass activity was obtained for $Pt_{13}Ru_{22}$ despite its 23 % lower surface activity compared to $Pt_{16}Ru_{14}$. This was explained by better Pt utilization of $Pt_{13}Ru_{22}$ compared to $Pt_{16}Ru_{14}$. This result demonstrated higher platinum utilization of the core shell structure and possible reduction of Pt loading with use of core–shell catalysts. The authors stated that further improvement can be achieved by enhancing Pt utilization with the highest surface activity and optimal PtRu ratio. This can be done by reducing Pt wt% while adjusting ruthenium wt% accordingly, in order to maintain the favorable surface Pt/Ru ratio.

Lin *et al.* [111] used a newly developed active screen plasma (ASP) technique to examine the effect of temperature and treatment duration on the growth of Pt nanowires on the GDL surface. They observed that starting from 100 °C temperature onwards, ECSA increased expressively, showing a maximum at 150 °C, and decreased before further increase of temperatures between 180 and 210 °C. The ECSA for samples treated at 150 °C was observed to be 65 % higher when compared with untreated one, indicating the influence of temperature on Pt nanowire growth.

Alcaide *et al.* [112] studied the influence of solvent on the catalyst inks for active layer manufacturing in DMFC applications. Two types of solvents, 2-propanol (IPA) and n-butyl acetate (NBA), have been used. The ECSA determined by CO stripping were 52.4 and 47.3 $m^2\ g^{-1}$, *i.e.* about 11 % greater ECSA was found for NBA than IPA. Results indicate that the ECSA of CL formulated with NBA was higher than that formulated with IPA. This clearly indicates that secondary pores in the catalyst formulated with NBA make accessible a greater surface area of the catalyst.

Using various novel catalyst support materials

Han *et al.* [113] tested the performance of DMFC anode with three different support materials. They prepared Pt-Ru electrocatalyst with acetylene black, Vulcan XC-72 and Ketjin Black EC-300J as carbon supports. They found small particle size, good dispersion and high methanol oxidation activity for Ketjin Black carbon support with 80 wt% Pt content, thus leading to higher ECSA and better Pt utilization. Pt-Ru supported on acetylene black has the lowest activity because of large clusters of nanoparticles caused by agglomeration. In contrast, Pt-Ru supported on Ketjen Black having better dispersion, exhibited three-fold increase in catalytic activity when compared to P-Ru/acetylene black.

Sun *et al.* [114] synthesized OMC-FT, OMC-F ordered mesoporous carbon with varying pore framework. Higher ECSA and good stability was observed for OMC-FT/Pt (62.96 $m^2\ g^{-1}$) than OMCs-F/Pt (54.36 $m^2\ g^{-1}$). Uniform dispersion of Pt nanoparticles resulted from high surface area and increased meso-porosity lead to high Pt utilization.

To avoid the waste of noble catalysts, Carmo *et al.* [115] used nitric acid incorporated carbon black support to prepare Pt/Ru electrocatalyst (PtRu/C-HNO_3). They observed better nano particle distribution on the catalyst support with high affinity and more exposed area of Ru towards species containing oxygen, leading to better ECSA of 104 $m^2\ g^{-1}$ with better Pt utilization.

Luo *et al.* [116] prepared a Pt-Nafion® high performance catalyst carbon support functionalized by perflourosulfonic acid and compared the results with Pt/O-C and Pt-Nafion®/C catalysts. They observed 30 % higher ECSA of 104.9 mg cm^{-2} for Pt-Nafion®/C catalyst when compared to Pt/O-C. The presence of Nafion® leads to higher dispersion of Pt nanoparticles and increased ECSA.

Liu *et al.* [117] used multi walled carbon nanotubes doped with phosphorous (P-MWCNT) as the catalyst support and prepared Pt/P-MWCNT electrode for DMFC. Improved Pt particles dispersion with increased intrinsic activity resulting in high Pt utilization was observed. This was attributed to change of charge density of P-MWCNT, leading to better interfacial interaction between surfaces of Pt and P-MWCNT.

(cc) BY

Sun *et al.* [118] designed and synthesized 1D open Pt structures with porous surface. Using polyelectrolyte-modified FeOOH nanorods as a template, they prepared hollow Pt nanotubes (PtNT). Employing the electrostatic attraction-based layer-by-layer assembly process, the self-supporting porous electrode was synthesized. ECSA of 19.6 $m^2 g^{-1}$ was observed for this electrode when compared to 16.8 $m^2 g^{-1}$ of Pt black catalyst. In spite of similar structure and composition of these electrodes, the increased ECSA was attributed to 1D porous structure of the prepared electrode.

Using chemical interfacial method, Gharibi *et al.* [119] prepared a composite of polyaniline (PANI) fiber doped with para-toluenesulfonic acid (PTSA) and fabricated the vulcan-polyaniline composite, C-PANI-PTSA. Pt electrocatalyst was deposited on the composite with different ratios (10, 15, 20, 25, 30 wt%), optimized and compared with Pt/C electrocatalyst. They found high ECSA (120.5 $m^2 g^{-1}$) for Pt/C-20 % PANI-PTSA electrocatalyst. C-PANI-PTSA composite exhibited better dispersion of Pt particles resulting in increased ECSA.

For depositing Pt nanoparticles, Li *et al.* [120] prepared a hybrid support $Ti_xSn_{1-x}O_2$-C *via* thermal method with substitution of Ti^{4+} by Sn^{4+} in TiO_2 lattice and observed improved Pt utilization with increased ECSA (68.9 $m^2 g^{-1}$) compared to the commercial catalyst.

Patel *et al.* [121] used the complexed sol-gel (CSG) process to synthesize Pt/Ru/TiN anode catalyst with titanium nitride (TiN) as the support. Higher ECSA of 59 $m^2 g^{-1}$ than the commercial catalyst was observed with uniform dispersion of Pt/Ru on the support. It was stated that the CSG process resulted in generation of the nanocrystalline Pt/Ru on the support.

Zhang *et al.* [122] used nitrogen-doped carbon nanotubes (CN_x-NTs) as the catalyst support material. They were prepared by carbonization of PPy-NT which were synthesized using methyl orange as a structure-guiding agent. ECSA values observed for these catalysts are 44.4 $m^2 g^{-1}$ (Pt/CN_x-NTs-600), 55.9 $m^2 g^{-1}$ (Pt/CN_x-NTs-700), 94.0 $m^2 g^{-1}$ (Pt/CN_x-NTs-800) and 71.2 $m^2 g^{-1}$ (Pt/CN_x-NTs-900). The highest catalytic activity of Pt/CN_x-NTs-800 catalyst is attributed to the optimal proportion of N-5, N-6 and N-Q.

Gao *et al.* [123] used graphene/Vulcan XC-72 carbon as the catalyst support and prepared platinum/graphene/Vulcan XC-72 (Pt/Gr-C) catalyst. Graphene oxide (GO) and H_2PtCl_6 were simultaneously reduced in ethylene glycol. Then, through ultra-sonication in aqueous solution, low-cost Vulcan XC-72 carbon was incorporated between graphene sheets. ECSA values of 37.9 $m^2 g^{-1}$ (Pt/C), 41.8 $m^2 g^{-1}$ (Pt/Gr) and 50.5 $m^2 g^{-1}$ (Pt/Gr-C), respectively were obtained. The best result for Pt/Gr-C was attributed to the inhibition effect of Vulcan XC-72 carbon sphere on the overlap of graphene and smaller particle size.

To increase the methanol oxidation activity of Pt catalyst, Jeon *et al.* [124] developed Pt/WC/C catalyst and analyzed electrochemical properties. CO-stripping studies revealed ECSA of 3.8 $m^2 g^{-1}$ for Pt/WC/C catalyst and 5.9 $m^2 g^{-1}$ for the conventional Pt/C. Higher ECSA (7.5 $m^2 g^{-1}$) was recorded for Pt/WC/C and not much different ECSA was observed for Pt/C (5.6 $m^2 g^{-1}$) when hydrogen adsorption method was used. Difference in ECSA observed by two methods was due to H^+ spill-over at the synthesized Pt/WC/C catalyst. Further, from CO stripping studies the reduced potential of 0.68 V for the synthesized catalyst Pt/WC/C than Pt/C (0.8 V) was found, indicating improved Pt/WC/C activity towards CO electro-oxidation.

Developing Pt metallic alloy and Pt-free catalysts

Giorgi *et al.* [125] deposited PtAu bimetallic nanoparticles on carbon nano fibers (CNF) directly grown on graphite paper and observed three times increase in the performance than for the commercial carbon support electrode having Pt utilization of 11 %. The augmented catalytic action of this

electrode when compared to PtRu catalyst was attributed to increased utilization of catalyst particles, which leads to superior ability towards methanol oxidation. The specific morphology of platelet CNF reduces amalgamation and regulates a robust foundation of catalyst nanoparticles on the substrate. In addition, the surface of the nanofibers is encompassed by functional groups which enable better oxidation, leading to the reduction of carbon-based species like CO that are accumulated on the electrode. Thereby Pt poisoning during cell operation is reduced and stability is enhanced.

Jang *et al.* [126] deposited Pt-Au alloy nanoparticles on graphene to prepare three-dimensional graphene electrodes (3D-GR/PtAu). Using the spraying and evaporation technique, Pt-Au alloy is deposited on colloidal graphene by employing the aerosol process. The ECSA (92 to 325 $m^2 g^{-1}$) values were found to increase with decrease in graphene oxide concentration (0.5 to 0.1 wt%). The highest ECSA of 325 $m^2 g^{-1}$ obtained for this electrode was relatively higher than for two-dimensional graphene electrode (2D-GR/PtAu) and commercially available Pt/C catalyst. This is attributed to increased active reaction sites, resulting in greater ability towards methanol oxidation.

Chang *et al.* [127-130] demonstrated anode catalyst for DMFC methanol electro oxidation using Ni_2P, CoP promoters. They synthesized Pt-Ni_2P, PtRu-Ni_2P, Pt-CoP and PtRu-CoP by Co-depositing Ni_2P, CoP promoters with Pt and PtRu on carbon support and optimized the electrodes by varying the amount of promoters (10, 20 30, 40 and 50 %). From H-adsorption and CO stripping measurements, they observed maximum ECSA for 30 % loading promoter for Pt-Ni_2P, Pt-CoP catalyst and 40 % loading of promoter for PtRu-Ni_2P and PtRu-CoP, respectively. The CV results are shown in Figure 9. The enhanced results were attributed to electron transfer between catalyst promoters and Pt, PtRu catalyst. The ECSA results are summarized in Table 10.

Table 10. *Platinum utilization analysis for DMFC anode*

GDE/structure/support/membrane/parameters	Pt loading, mg cm^{-2}	ECSA, $m^2 g^{-1}$	Ref.
Nano-Nafion® membrane	4	11.5	[107]
Ionomer coating (5 wt%)	40 wt%	63.0	[108]
Roughness Factor(RF)	1.0	45.8	[109]
Atomic ratio	0.7	35	[110]
Plasma treatment conditions	-	25.8	[111]
Effect of solvent:	0.8	52.4	[112]
P-Ru/Ketjen Blank	5	45.63	[113]
Ordered mesoporous carbon	20 wt%	62..96	[114]
Nitric acid functionalized CB/Vulcan XC72R-HNO_3	20 wt%	104	[115]
Nafion® functionalized CB (Pt/Nafion®-C)	20 mg	104.9	[116]
Phosphorous doped CNT(Pt/P-MWCNT)	-	78.9	[117]
1D open - Pt structures with porous surface(PtNTs)	0.028	19.6	[118]
Pt/C-PANI-PTSA	0.1	120	[119]
SnO_2-TiO_2	1	68.9	[120]
Nanostructures TiN	0.3	59	[121]
Pt/CNx-NTS-800	5.3 wt%	94.0	[122]
Pt/Gr-C	0.019	50.5	[123]
Pt/WC/C	-	3.8	[124]
Platelet Carbon Nano fiber grown on graphite paper.	0.011	59	[125]
3D-GR/PtAu	20 wt%	325	[126]
Pt-Ni_2P-30 %	5	69	[127]
PtRu-Ni_2P-40 %	2	113	[128]
Pt-CoP-30 %	0.3	81	[129]
PtRu-CoP-40 %	2	116	[130]

(cc) BY

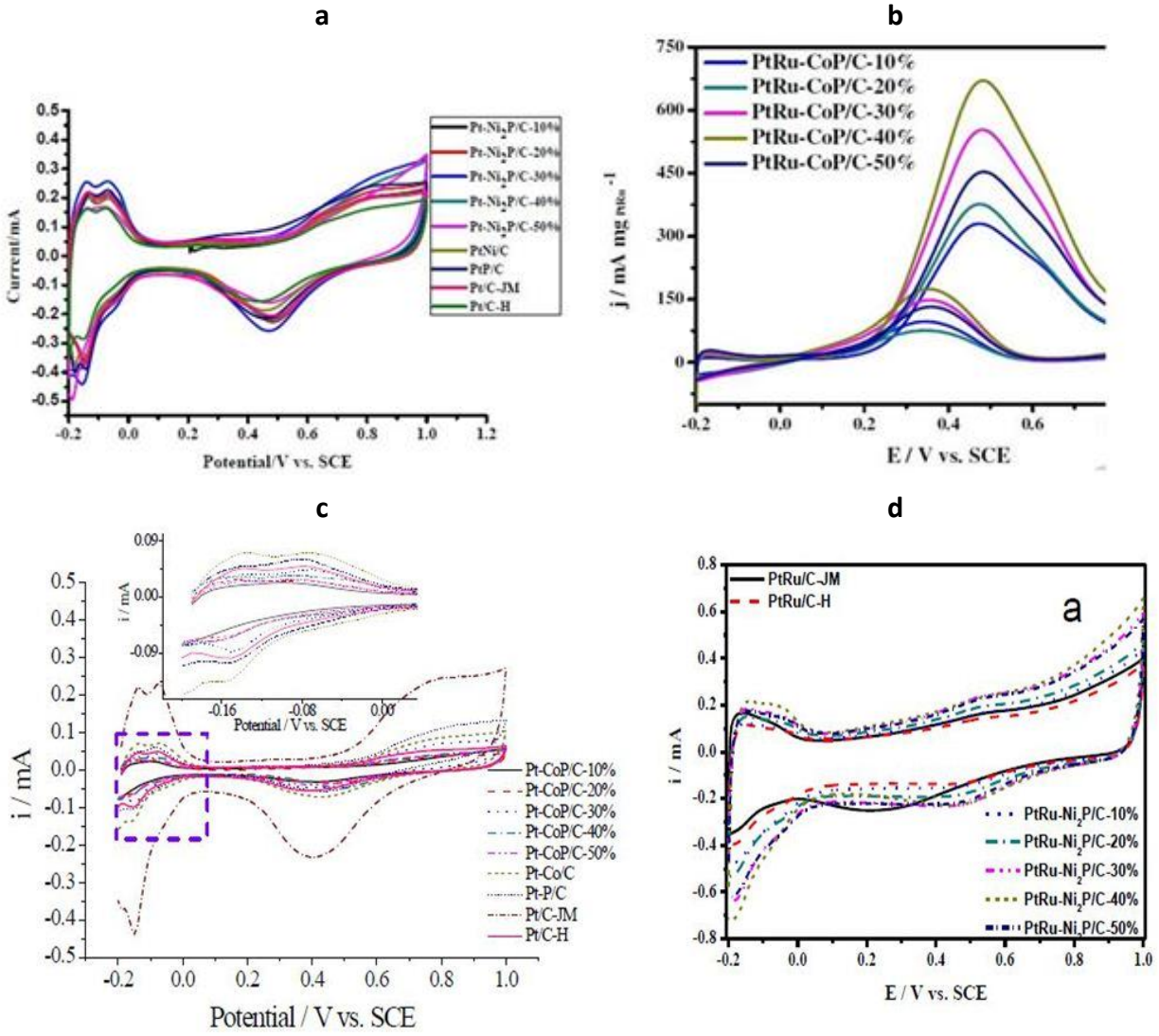

Figure 9. *Cyclic voltammograms of (a) Pt-Ni_2P (b) PtRu-CoP/C (c) Pt-CoP/C (d) PtRu-Ni_2P for varying amount of promoters (10, 20, 30, 40 and 50 %).*

Conclusion

This review has summarized various approaches adopted by researches over the past two decades to enhance Pt utilization efficiency and thereby reduce cost and address various other technical barriers for PEMFC's and DMFC's to become commercially viable. It is established that catalysis is a surface phenomenon on electrodes, where catalyst activity is largely governed by the dispersion of particles, particle size and the exposed percentage of particles available in the catalyst layer. For this reason, and in order to reduce Pt loading, it is essential that efforts must be made to use all Pt particles during reaction. Reducing particle size can therefore be seen as the primary focus of research so far in the area of catalyst utilization.

It is well known that the exposed percentage of the catalyst available for catalytic activity is the reciprocal of particle size. This means that reducing the particle size to below 1 nm levels may lead to 100 % Pt utilization. However, research revealed that the porous structure of the carbon support with the pore size at approximately 2 nm is a hindrance. That is, reduction of Pt particle size below 2 nm lowers its specific activity and results in the pocketing of the particles inside the porous structure of the carbon support, rendering them inaccessible for catalyst reaction. Further, the behavior of metal particles smaller than 1 nm display greater interaction with the carbon support in deviation of their normal conventional behavior thereby reducing their participation in electroactivity.

Nevertheless, the recent progress in catalyst utilization research has brought down the effective particle size of platinum-based catalyst to about 2-4 nm range and the percentage of exposed Pt particles to the range of 20-50 %. This has been achieved through the following means:

- Increasing of TPB, where electrolyte, electrode and fuel gas come into contact with each other, by optimizing the composition of the catalyst layer and catalyst distribution.
- Attainment of reduced mass transport losses by controlling pore structure and hydrophobicity especially at high current density of CL to provide more electrochemical reaction area with improved gas and liquid transport pathways.
- Reducing of the interfacial resistance by tailoring CL and GDL, and between CL and membrane interfacial structures
- Designing novel methods for ordered CL preparation.

As it was established that reducing the particle size may not result in optimizing catalyst utilization, other viable alternatives need to be explored. In addition to the use of Pt and Pt alloy as a catalyst, efforts are also being carried out to investigate the application of non-Pt alloys as catalysts to reduce the overall cost of the fuel cell.

Also, it is worth mentioning here that recent research indicates stability or the life span of PEMFC as the most important factor, irrespective of Pt loading per area. This means that as long as high Pt loading contributes to increase in stability, life span and the overall effectiveness of the fuel cell, a reduction of Pt loading should not be prioritized. Nevertheless, development of Pt electrocatalyst with low Pt loading will continue to stay in the focus of active research.

NOMENCLATURE

1D	one dimensional
ASP	active screen plasma
AST	accelerated stress test
AuPt	gold nanoparticles supporting Pt
BH	borohydride
BP	black pearl
CA	carbon aerogels
CB	carbon black
CCL	cathode catalyst layer
CCS	catalyst coated substrate
CC	carbon cloth
CCS-20	compound carbon support
CL	catalyst layer
CMK	a family of mesoporous material
CMPL	carbon microporous layer
CNF	carbon nanofibers
CNT	carbon nanotubes
CO_{ad}	adsorbed carbon monoxide
CP	carbon paper
CTAB	centyl trimethyl ammonia bromide
CV	cyclic voltammetry
CVD	chemical vapor deposition
CXG	carbon xerogels
DCL	double catalyst layer
DC	direct current
DMFC	direct methanol fuel cell
DPC	doped porous carbon
E/E	electrospinning and electrospraying
HD-EG	homogeneous deposition of ethylene glycol
HGS	hollow graphitized carbon spheres
IE	ion-exchange
IPA	isopropyl alcohol
LSV	linear sweep voltammetry
MEA	membrane electrode assembly
mPAD	modified polymer-assisted deposition
MPL	microporous layer
MWCNT	multiwalled carbon nanotubes
N/C	Nafion® carbon ratio
$NaBH_4$	sodium borohydride
NCS	novel cathode structure
NDCL	novel double catalyst layer
NMP	N-Methyl-2-pyrrolidoone
OMC	ordered mesoporous carbon
ORR	oxygen reduction reaction
PEMFC	proton exchange membrane fuel cell
PGM	platinum group metal
PLD	pulse laser deposition technique
PPT	pulse plating technique
PtUt	platinum utilization
PTFE	poly tetra flouro ethylene
PtNP	platinum nanoparticles
PtNT	platinum nanotubes
PTSA	para sulfonic acid
rGO	reduced graphene oxide
$ScCO_2$	super critical carbon dioxide
SCL	single catalyst layer

(cc) BY

ECSA	electrochemical active surface area	SDS	sodium dodecyl sulphate
EG	ethylene glycol	SENS	surface enriched nanosized
FGS	functionalized graphene sheets	SWCNT	single walled carbon nanotubes
GDE	gas diffusion electrode	TCS	traditional catalyst structure
GDL	gas diffusion layer	TFCL	thin film catalyst layer
GO	graphene oxide	TPB	triple phase boundary
Gr	graphene	UPCF	ultrafine porous carbon fibre
GSA	geometrical specific surface area	HUPD	hydrogen under potential deposition

References

[1] C. Berger, *Handbook of Fuel Cell Technology*, Prentice-Hall, NJ, United States, 1968.

[2] T. Zhao, C. Xu, Fuel cells: direct methanol fuel cell: overview performance and operational conditions, J. Garche, Oxford: Elsevier, Amsterdam, 2009, p.381–389.

[3] S. J. Peighambardoust, S. Rowshanzamir, M. Amjadi, *International Journal of Hydrogen Energy* **35** (2010)9349-84.

[4] V. Mehta, J. S. Cooper, *Journal of Power Sources* **114** (2003) 32-53.

[5] K. V. Schaller, C. Gruber, *Fuel Cells Bulletin* **3** (2000) 9-13.

[6] F. Panik, *Journal of Power Sources* **71** (1998) 36-8.

[7] K. Sopian , W. R. Daud, *Renewable Energy* **31** (2006) 719- 27.

[8] S. Litster, G. McLean, *Journal of Power Sources* **130** (2004) 61-76.

[9] Z. Liu, L. Ma, J. Zhang, K. Hongsirikarn, J. G. Goodwin, *Catalysis Reviews* **55** (2013) 255-88.

[10] I.E. Stephens, A. S. Bondarenko, U. Grønbjerg, J. Rossmeisl, I. Chorkendorff, *Energy and Environmental Science* **5** (2012) 6744-62.

[11] U.S. Dept. of Energy. Fuel cell hand book, 7th ed., West Virginia: Office of Fossil Fuel, *National Energy Technology Laboratory*; October 2000.

[12] De Frank Bruijn, G.J. Janssen, *PEM fuel cell materials: Costs, performance and durability.* Springer, New York, 2013, p. 249-303.

[13] A.Lavacchi, H. Miller,F. Vizza, *Nanotechnology in electrocatalysis for energy*, Springer, New York,2013.

[14] M. S. Wilson, S. Gottesfeld, *Journal Applied Electrochemistry* **22**(1992) 1-7.

[15] C.H. Hsu, C.C. Wan, *Journal of Power Sources* (2003) 268-73.

[16] G. S. Kumar, M. Raja, S. Parthasarathy, *Electrochimica Acta* **40** (1995) 285-90.

[17] D. Thompsett, Catalysts for the proton exchange membrane fuel cell, *Fuel cell technology handbook.* 2003.

[18] Y. Yi, B. D. Lee, S. K. Kim, D. H. Jung, E.M. Jung, S. M. Hwang, S. Y. Choi, D. H. Peck, *Journal of Electrochemical Science* **11** (2016) 5909-23

[19] J. Zeng, J.Y. Lee, W. Zhou*, Applied Catalysis A: General* **308** (2006) 99-104.

[20] U.A. Paulus, Z. Veziridis, B. Schnyder, M. Kuhnke, G.G. Scherer, A. J. Wokaun, *Journal of Electroanalytical Chemistry* **541** (2003) 77-91.

[21] M. Łukaszewski, M. Soszko, A. Czerwiński, *International Journal of Electrochemical Science* **11** (2016) 4442-69.

[22] T. Binninger, E. Fabbri, R. Kötz, T.j. Schmidt, *Journal Electrochemical Society* **61** (2014) H121-8.

[23] A. Pozio, M. De Francesco, A. Cemmi , F. Cardellini, L. Giorgi, *Journal of Power Sources* **105** (2002) 13-9.

[24] M. A. Watanabe, S.Motoo, *Journal of Electroanalytical Chemistry and Interfacial Electrochemistry* **60** (1975) 267-73.

[25] H. A. Gasteiger, W.Gu, R. Makharia, M. F. Mathias, B. Sompalli, Beginning-of-life MEA performance—efficiency loss contributions, *Handbook of fuel cells* 2003.

[26] T. Vidaković, M. Christov, K. Sundmacher, *Electrochimica Acta* **18** (2007) 5606-13.

[27] D. F. Van der Vliet, C. Wang, D. Li, A. P. Paulikas, J. Greeley, R. B. Rankin, D. Strmcnik, D. Tripkovic, N. M. Markovic, V. R. Stamenkovic, *Angewandte Chemie* **124** (2012) 3193-6.

[28] S. Gamburzev, C. Boyer, A.J. Appleby, *Fuel Cells Bulletin* **2** (1999) 6-8.

[29] S. Martin, J.L. Castillo, *International Journal of Hydrogen Energy* **35** (2010) 10446–10451.
[30] S. Martin, P. L. Garcia-Ybarra, J. L. Castillo, *Journal of Power Sources* **195** (2010) 2443-9.
[31] S. Martin, B. Martinez-Vazquez, P.L. Garcia-Ybarra, J.L. Castillo, *Journal of Power Sources* **229** (2013) 179–184.
[32] X. Wang, F.W. Richey, K.H. Wujcik, Y. A. Elabd, *Journal of Power Sources* **264** (2014) 42–48.
[33] S.M. Alia, G. Zhang, D. Kisailus, D. Li, S. Gu, K. Jensen, Y. Yan, *Advanced Functional Materials* **20** (2010) 3742-3746
[34] H. Su, T. Jao, O. Barron, B.G. Pollet, S. Pasupathi, *Journal of Power Sources* **267** (2014) 155–159.
[35] Y. Nabil, S. Cavaliere, I. A. Harkness, J. D. Sharman, D. J. Jones, J. Rozière, *Journal of Power Sources* **363** (2017) 20-26.
[36] Y. Nabil-Moreau, S. Cavaliere, I. Harkness, G. Hards, J. Sharman, D. J. Jones, J. Rozière, *ECS Transactions* **69** (2015) 1221-1226.
[37] A. Esmaeilifar, S. Rowshanzamir,M.H. Eikani, E. Ghazanfari, *Energy* **35** (2010) 3941-57.
[38] A. Smirnova, U. Kitkamthorn, M. Aindow, T. Lemi, *Journal of Power Sources* **179** (2008) 532–540.
[39] B. Fang, N.K. Chaudhari, M. Kim, J.H. Kim, J. Yu, *Journal of American Chemical Society* **131** (2009) 15330–15338.
[40] W. Mróz, B. Budner, W. Tokarz, P. Piela, M.L. Korwin-Pawlowski, *Journal of Power Sources* **273** (2015) 885–893.
[41] U. Rost, R. Muntean, G. Marginean, C. Merino, R. Diez, N. Vaszilcsin, M. Brodmann, *International Journal of Electrochemical Science* **11** (2016) 9110–9122.
[42] R. H. Huang, W.K. Chao, R. S. Yu, K. L. Hsueh, F. S. Shieu, *Journal of Power Sources* **205** (2012) 93–99.
[43] H. Lv, S. Mu, N.Cheng, M. Pan, *Applied Catalysis B: Environmental* **100** (2010) 190-196.
[44] S. Sharma, B.G.Pollet, *Journal of Power Sources* **208** (2012) 96-119.
[45] H. Su, S. Liao, Y. Wu, *Journal of Power Sources* **195** (2010) 3477–3480.
[46] Y. Qiu, H. Zhang, H. Zhong, F. Zhang, *International Journal of Hydrogen Energy* **38** (2013) 5836–5844.
[47] G.S. Avcioglu, B. Ficicilar, A. Bayrakceken, I. Eroglu, *International Journal of Hydrogen Energy* **40** (2015) 7720–7731.
[48] M. Breitwieser, M. Klingele, B. Britton, S. Holdcroft, R. Zengerle, S. Thiele, *Electrochemistry Communications* **60** (2015) 168-71.
[49] D. Kaplan, M. Goor, M. Alon, S. Tsizin, L. Burstein, Y. Rosenberg, I. Popov, E. Peled, *Journal of Power Sources* **306** (2016) 219–225.
[50] G.Y. Chen, C. Wang, Y.J. Lei, J. Zhang, Z. Mao, Z.Q. Mao, J.W. Guo, J. Li, M. Ouyang, *International Journal of Hydrogen Energy* **42** (2017) 29960–29965.
[51] M. Yaldagard, M. Jahanshah, N. Seghatoleslami, *World Journal of Nano Science and Engineering* **3** (2014) 121.
[52] X. Cheng, B. Yi, M. Han, J. Zhang, Y. Qiao, J. Yu, *Journal of Power Sources* **79** (1999) 75–81.
[53] E. Antolini, L. Giorgi, A. Pozio, E. Passalacqua, *Journal of Power Sources* **77** (1999) 136–142.
[54] G. Sasikumar, J.W. Ihm, H. Ryu, *Journal of Power Sources* **132** (2004) 11–17.
[55] J. Jiang, B. Yi, *Journal of Electroanalytical Chemistry* **577** (2005) 107–115.
[56] A. Bayrakceken, A. Smirnova, U. Kitkamthorn, M. Aindow, L. Turker, I. Eroğlu, C. Erkey, *Chemical Engineering Communications* **196** (2009) 194–203.
[57] A. Khan, B.K. Nath, J. Chutia, *Electrochimica Acta* **146** (2014) 171–177.
[58] E. Slavcheva, G. Ganske, G. Topalov, W. Mokwa, U. Schnakenberg, *Applied Surface Science* **255** (2009) 6479–6486.
[59] X. Wang, F.W. Richey, K.H. Wujcik, R. Ventura, K. Mattson, Y.A. Elabd, *Electrochimica Acta* **139** (2014) 217–224.
[60] J. Speder, A. Zana, I. Spanos, J.J.K. Kirkensgaard, K. Mortensen, M. Hanzlik, M. Arenz, *Journal of Power Sources* **261** (2014) 14–22.
[61] G. Zhao, T.S. Zhao, J. Xu, Z. Lin, X. Yan, *International Journal of Hydrogen Energy* **42** (2017) 3325–3334.
[62] T.H. Kim, J.Y. Yi, C.Y. Jung, E. Jeong, S.C. Yi, *International Journal of Hydrogen Energy* **42** (2017) 478–485.
[63] C. Ruengkit, N. Tantavichet, *Thin Solid Films* **636** (2017) 116–126.

(cc) BY

[64] A. Egetenmeyer, I. Radev, D. Durneata, M. Baumgärtner, V. Peinecke, H. Natter, R. Hempelmann, *International Journal of Hydrogen Energy* **42** (2017) 13649–13660.
[65] D. Zhao, B. Q. Xu, *Angewandte Chemie International Edition* **45** (2006) 4955-4959.
[66] A. Kongkanand, S. Kuwabata, G. Girishkumar, P. Kamat, *Langmuir* **22** (2006) 2392–2396.
[67] A. Orfanidi, M.K. Daletou, S.G. Neophytides, *Applied Catalysis B: Environmental* **106** (2011) 379–389.
[68] W. Zhu, D. Ku, J.P. Zheng, Z. Liang, B. Wang, C. Zhang, S. Walsh, G. Au, E.J. Plichta, *Electrochimica Acta* **55** (2010) 2555–2560.
[69] R. Kou, Y. Shao, D. Wang, M.H. Engelhard, J.H. Kwak, J. Wang, V. V. Viswanathan, C. Wang, Y. Lin, Y. Wang, I.A. Aksay, J. Liu, *Electrochemistry Communications* **11** (2009) 954–957.
[70] E. Salernitano, L. Giorgi, T. Dikonimos, *International Journal of Hydrogen Energy* **39** (2014) 15005–15016.
[71] S. Huang, P. Ganesan, B.N. Popov, *Applied Catalysis B: Environmental* **102** (2011) 71–77.
[72] J. Song, G. Li, J. Qiao, *Electrochimica Acta* **177** (2015) 174-180.
[73] L. I. Sanli, V. Bayram, S. Ghobadi, N. Duzen, S A Gursel, *International Journal of Hydrogen Energy* **42** (2017) 1085–1092.
[74] R. Singh, M.K. Singh, S. Bhartiya, A. Singh, D.K. Kohli, P.C. Ghosh, S. Meenakshi, P.K. Gupta, *International Journal of Hydrogen Energy* **42** (2017) 11110–11117.
[75] O. Lori, S. Gonen, L. Elbaz, *Journal of Electrochemical Society* **164** (2017) F825–F830.
[76] A. Ignaszak, C. Song,W. Zhu, J. Zhang, A. Bauer, R. Baker, V. Neburchilov, S. Ye, S. Campbell. *Electrochimica Acta* **69** (2012) 397-405.
[77] J.Lobato, H. Zamora, J. Plaza, P. Cañizares, M. A. Rodrigo, *Applied Catalysis B: Environmental* **198** (2016) 516-524.
[78] S. Shahgaldi, J. Hamelin, *Fuel* **150** (2015) 645-655.
[79] L. Borchardt, F. Hasché, M. R. Lohe, M. Oschatz, F. Schmidt, E. Kockrick, C. Ziegler,T. Lescouet, B. Büchner, D. Farrusseng, *Carbon* **50** (2012) 1870.
[80] H.A.Gasteiger, S.S. Kocha , B. Sompalli, F.T. Wagner, *Applied Catalysis B: Environmental* ***56*** (2005) 9-35.
[81] B. Wang, *Journal of Power Sources* **152** (2005) 1-5.
[82] H. Wu, D. Wexler, H. Liu, *Material Chemistry Physics* **136** (2012) 845–849.
[83] M. Sahoo, S. Ramaprabhu, *Energy* **119** (2017) 1075–1083.
[84] C. Wang, Z. Lin Chen, A. Wen Tao, H. Zhang, *Journal of Electrochemical Energy Conversion and Storage* **13** (2016) 21001.
[85] S. Koh, N. Hahn, C. Yu, P. Strasser, Journal of *Electrochemical Society* **12** (2008) B1281-8.
[86] M. Bele, P. Jovanovič, A. Pavlišič, B. Jozinović, M. Zorko, A. Rečnik, E. Chernyshova, S. Hočevar, N. Hodnik, M. Gaberšček, *Chemical Communications* **50** (2014) 13124-6.
[87] P. Mani, R. Srivastava, P. Strasser, *Journal of Physical Chemistry C* **112** (2008) 2770-8.
[88] S. Hong, M. Hou, H. Zhang, Y. Jiang, Z. Shao, B. Yi, *Electrochimica Acta* **245** (2017) 403–409.
[89] S. Wang, G. Sun, Z. Wu, Q. Xin, *Journal of Power Sources* **165** (2007) 128–133.
[90] D.J. You, K. Kwon, S.H. Joo, J.H. Kim, J.M. Kim, C. Pak, H. Chang, *International Journal of Hydrogen Energy* **37** (2012) 6880–6885.
[91] Z.F. Wang, L. Shi, G.Z. Gou, A.P. Fan, C. Xu, L. Zhang, In Advanced Materials and Structural Engineering: *Proceedings of the International Conference on Advanced Materials and Engineering Structural Technology (ICAMEST 2015*), April 25-26, 2015, Qingdao, China, p. 167. CRC Press, 2016.
[92] L. Pu, H. Zhang, T. Yuan, Z. Zou, L. Zou, X.-M. Li, H. Yang, *Journal of Power Sources* **276** (2015) 95–101.
[93] B. Krishnamurthy, S. Deepalochani, K.S. Dhathathreyan, *Fuel Cells* **8** (2008) 404–409.
[94] B. Krishnamurthy, S. Deepalochani, *International Journal of Hydrogen Energy* **34** (2009) 446–452.
[95] B. Krishnamurthy, S. Deepalochani, *Journal of Electrochemical Society* **4** (2009) 386–395.
[96] S. Matar, H. Liu, *Electrochimica Acta* **56** (2010) 600–606.
[97] Q. Jiang, Z. Peng, X. Xie, K. Du, G. Hu, Y. Liu, *Transactions of Nonferrous Metals Society of China* **21** (2011) 127–132.
[98] A.D. Moore, S.M. Holmes, E.P.L. Roberts, *RSC Advances* **2** (2012) 1669–1674.
[99] X. Zhao, W. Li, Y. Fu, A. Manthiram, *International Journal of Hydrogen Energy* **37** (2012) 9845-9852.

[100] J.J. Wang, G.P. Yin, J. Zhang, Z.B. Wang, Y.Z. Gao, *Electrochimica Acta* **52** (2007) 7042–7050.
[101] C. Chen, C. Chen, C. Chen, F. Chuang, *Electrochemistry Communications* **9** (2007) 159–163.
[102] M. Yaldagard, M. Jahanshahi, N. Seghatoleslami, *Applied Surface Science* **317** (2014) 496–504.
[103] R.I. Jafri, N. Rajalakshmi, K.S. Dhathathreyan, S. Ramaprabhu, *International Journal of Hydrogen Energy* **40** (2015) 4337–4348.
[104] C. Alegre, D. Sebastián, M.E. Gálvez, R. Moliner, M.J. Lázaro, *Applied Catalysis B: Environmental* **192** (2016) 260–267.
[105] T. Tesfu-Zeru, M. Sakthivel, J.F. Drillet, *Applied Catalysis B: Environmental* **204** (2017) 173–184.
[106] M.G. Hosseini, R. Mahmoodi, *International Journal of Hydrogen Energy* **42** (2017) 10363–10375.
[107] Z.X. Liang, T.S. Zhao, *Journal of Physical Chemistry* **111** (2007) 8128–8134.
[108] M.A. Scibioh, I. Oh, T. Lim, S. Hong, H.Y. Ha, *Applied Catalysis B: Environmental* **77** (2008) 373-385.
[109] L. Pu, J. Jiang, T. Yuan, J. Chai, H. Zhang, Z. Zou, X.M. Li, H. Yang, *Applied Surface Science* **327** (2015) 205–212.
[110] D. Kaplan, L. Burstein, I. Popov, E. Peled, *Journal of Electrochemical Society* **163** (2016) F1004–F1010.
[111] K. Lin, Y. Lu, S. Du, X. Li, H. Dong, *International Journal of Hydrogen Energy* **41** (2016) 7622–7630.
[112] F. Alcaide, G. Álvarez, P.L. Cabot, R. Genova-Koleva, H.J. Grande, O. Miguel, *Electrochimica Acta* **231** (2017) 529–538.
[113] K. Han, J. Lee, H. Kim, *Electrochimica Acta* **52** (2006) 1697–1702.
[114] Z.-P. Sun, X.-G. Zhang, Y.-Y. Liang, H. Tong, R.L. Xue, S.D. Yang, H.-L. Li, *Journal of Electroanalytical Chemistry* **633** (2009) 1–6.
[115] M. Carmo, M. Linardi, *Applied Catalysis A: General* **355** (2009) 132–138.
[116] F. Luo, S. Liao, D. Chen, *Journal of Energy Chemistry* **22** (2013) 87–92.
[117] Z. Liu, Q. Shi, F. Peng, H. Wang, R. Zhang, H. Yu, *Electrochemistry Communications* **16** (2012) 73–76.
[118] H. Sun, L. Qi, X. Jiang, G. Fu, L. Xu, D. Sun, Z. Gu, Y. Tang, *New Journal of Chemistry* **41** (2017).
[119] H. Gharibi, M. Amani, H. Pahlavanzadeh, M. Kazemeini, *Electrochimica Acta* **97** (2013) 216–225.
[120] Y. Li, C. Liu, Y. Liu, B. Feng, L. Li, H. Pan, W. Kellogg, D. Higgins, G. Wu, *Journal of Power Sources* **286** (2015) 354–361.
[121] P.P. Patel, M.K. Datta, P.H. Jampani, D. Hong, J.A. Poston, A. Manivannan, P.N. Kumta, *Journal of Power Sources* **293** (2015) 437–446.
[122] L. M. Zhang, X. L. Sui, L. Zhao, J.J. Zhang, D. M. Gu, Z. B. Wang, *Carbon* **108** (2016) 561–567.
[123] H. Gao, L. He, Y. Zhang, S. Zhang, L. Wang, *Ionics (Kiel)* **23** (2017) 435–442.
[124] M. K. Jeon, K. R. Lee,W. S. Lee, H. Daimon, A. Nakahara, S. I. Woo, *Journal of Power Sources* **185** (2008) 927-931.
[125] L. Giorgi, E. Salernitano, T. D. Makris, S. Gagliardi, V. Contini, M. De Francesco, *International Journal of Hydrogen Energy* **39** (2014) 21601–21612.
[126] H. D. Jang, S. K. Kim, H. Chang, J. Choi, B. Cho, E. Hee, J. Choi Huang, *Carbon* **93** (2015) 869-877.
[127] J. Chang, L. Feng, C. Liu , W. Xing, X. Hu, *Energy & Environmental Science* **7** (2014) 1628-1632.
[128] J. Chang, L. Feng, C. Liu, W. Xing, *ChemSusChem* **8** (2015) 3340-3347.
[129] J. Chang, L. Feng, K. Jiang, H. Xue, W. B. Cai, C. Liu, W. Xing, *Journal of Materials Chemistry* A **47** (2016) 18607-18613.
[130] L. Feng, K. Li, J. Chang, C. Liu, W. Xing, *Nano Energy* **15** (2015) 462-9.

©2019 by the authors; licensee IAPC, Zagreb, Croatia. This article is an open-access article distributed under the terms and conditions of the Creative Commons Attribution license (http://creativecommons. org/licenses/by/4.0/)